Article

Aberrant H3K4me3 modification of epiblast genes of extraembryonic tissue causes placental defects and implantation failure in mouse IVF embryos

Graphical abstract
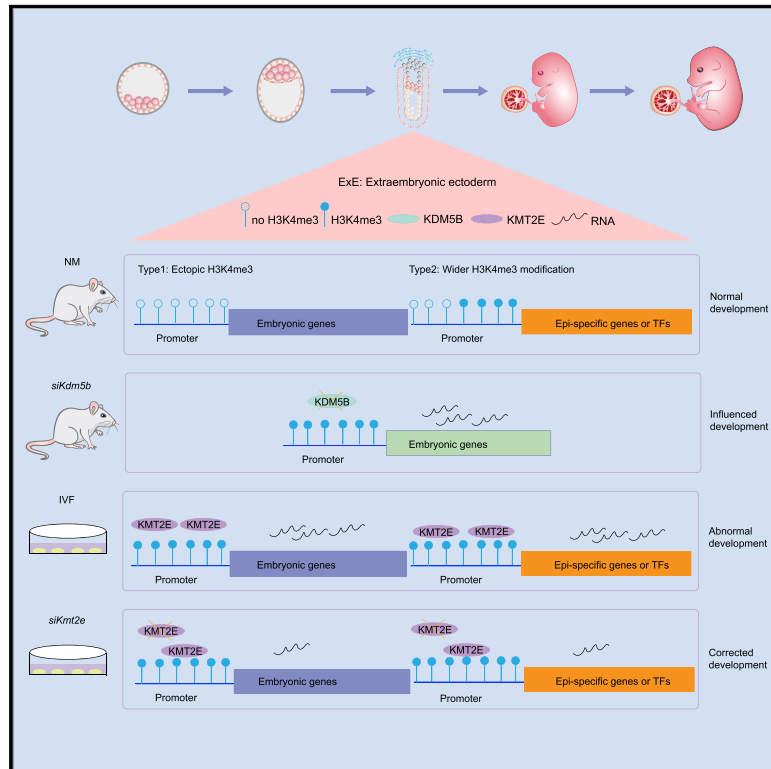
Authors

Dandan Bai, Jin Sun, Chuan Chen, ..., Cizhong Jiang, Shaorong Gao, Wenqiang Liu

Correspondence

czjiang@tongji.edu.cn (C.J.), gaoshaorong@tongji.edu.cn (S.G.), liuwenqiang@tongji.edu.cn (W.L.)

In brief

Bai et al. show that IVF manipulation disrupts extraembryonic ectoderm (ExE) gene expression and placental development. Aberrant histone H3K4me3 in ExE is an important cause for embryo implantation failure and extraembryonic developmental abnormalities. *Kmt2e* knockdown improves the development of IVF embryos and reduces abnormal gene expression in ExE.

Highlights

- IVF affects implantation, extraembryonic ectoderm (ExE), and placental development

- IVF disrupts extraembryonic tissue-specific gene expression in ExE

- Aberrant H3K4me3 in ExE causes gene expression and developmental defects

- *Kmt2e* knockdown improves the development of IVF embryos

CellPress

Cell Reports

Article

Aberrant H3K4me3 modification of epiblast genes of extraembryonic tissue causes placental defects and implantation failure in mouse IVF embryos

Dandan Bai,[1,3] Jin Sun,[1,2,3] Chuan Chen,[1] Yanping Jia,[1] Yanhe Li,[1] Kuisheng Liu,[1] Yalin Zhang,[1] Jiqing Yin,[1] Yingdong Liu,[1] Xiaoxiao Han,[1] Jingling Ruan,[1] Xiaochen Kou,[1] Yanhong Zhao,[1] Hong Wang,[1] Zheng Wang,[1] Miaoxin Chen,[1] Xiaoming Teng,[1] Cizhong Jiang,[1,2,*] Shaorong Gao,[1,4,*] and Wenqiang Liu[1,*]

[1]Shanghai Key Laboratory of Maternal Fetal Medicine, Clinical and Translational Research Center of Shanghai First Maternity and Infant Hospital, Shanghai Key Laboratory of Signaling and Disease Research, Frontier Science Center for Stem Cell Research, School of Life Sciences and Technology, Tongji University, Shanghai 200092, China
[2]Key Laboratory of Spine and Spinal Cord Injury Repair and Regeneration of Ministry of Education, Orthopaedic Department of Tongji Hospital, School of Life Sciences and Technology, Tongji University, Shanghai 200092, China
[3]These authors contributed equally to this work
[4]Lead contact
*Correspondence: czjiang@tongji.edu.cn (C.J.), gaoshaorong@tongji.edu.cn (S.G.), liuwenqiang@tongji.edu.cn (W.L.)
https://doi.org/10.1016/j.celrep.2022.110784

SUMMARY

Assisted reproductive technology has been widely applied in the treatment of human infertility. However, accumulating evidence indicates that *in vitro* fertilization (IVF) is associated with a low pregnancy rate, placental defects, and metabolic diseases in offspring. Here, we find that IVF manipulation notably disrupts extraembryonic tissue-specific gene expression, and 334 epiblast (Epi)-specific genes and 24 Epi-specific transcription factors are abnormally expressed in extraembryonic ectoderm (ExE) of IVF embryos at embryonic day 7.5. Combined histone modification analysis reveals that aberrant H3K4me3 modification at the Epi active promoters results in increased expression of these genes in ExE. Importantly, we demonstrate that knockdown of the H3K4me3-recruited regulator *Kmt2e*, which is highly expressed in IVF embryos, greatly improves the development of IVF embryos and reduces abnormal gene expression in ExE. Our study therefore identifies that abnormal H3K4me3 modification in extraembryonic tissue is a major cause of implantation failure and abnormal placental development of IVF embryos.

INTRODUCTION

Infertility has developed into a severe societal problem around the world. The total number of infertile couples worldwide has been estimated at 48.5 million, accounting for 8% to 12% of childbearing-aged couples (Mascarenhas et al., 2012; Vander Borght and Wyns, 2018). The birth and continuous improvement of assisted reproductive technology (ART) have provided an effective treatment for the decline in population fertility. *In vitro* fertilization (IVF) is the commonly used ART procedure, involves mainly superovulation, sperm processing, fertilization, and *in vitro* culture. Recently, an increasing number of studies have shown that IVF-derived offspring have short-term and long-term health problems, including pregnancy loss, placental abnormalities, low birth weight, and metabolic diseases (Guo et al., 2017; Hansen, 2020; Hu et al., 2018; Jauniaux et al., 2020; von Wolff and Haaf, 2020). Epigenetic modifications, including DNA methylation and histone modifications, play important roles in embryo development and disease initiation. Further research has found that IVF changes the epigenetic inheritance of the offspring, resulting in a gene expression pattern

that is different from that of naturally conceived offspring (Ventura-Junca et al., 2015). Extraembryonic tissues exhibit enhanced susceptibility to these influences and play a decisive role in implantation. After implantation, extraembryonic tissues (mainly placenta) play an important role in the balance of maternal-fetal nutrition distribution and determine fetal development. At present, although a large number of studies have confirmed that IVF can lead to placental defects, such as increased placental weight, reduced efficiency, and structural disorders, the specific mechanism remains largely elusive (Bloise et al., 2012; de Waal et al., 2015; Tan et al., 2016).

The establishment of correct epigenetic modification in the trophectoderm (TE) is essential for embryo implantation and placental development. H3K4me3 modifications, especially broad H3K4me3 domains, mark cell-specific genes and transcription factors in preimplantation embryos and in a given cell type (Chen et al., 2015; Dahl et al., 2016; Liu et al., 2016; Park et al., 2020). Some reports have revealed that bivalent (H3K4me3 and H3K27me3) states established during embryonic development play very important roles in cell lineage differentiation and the formation of tissues and organs (Huang et al., 2015;
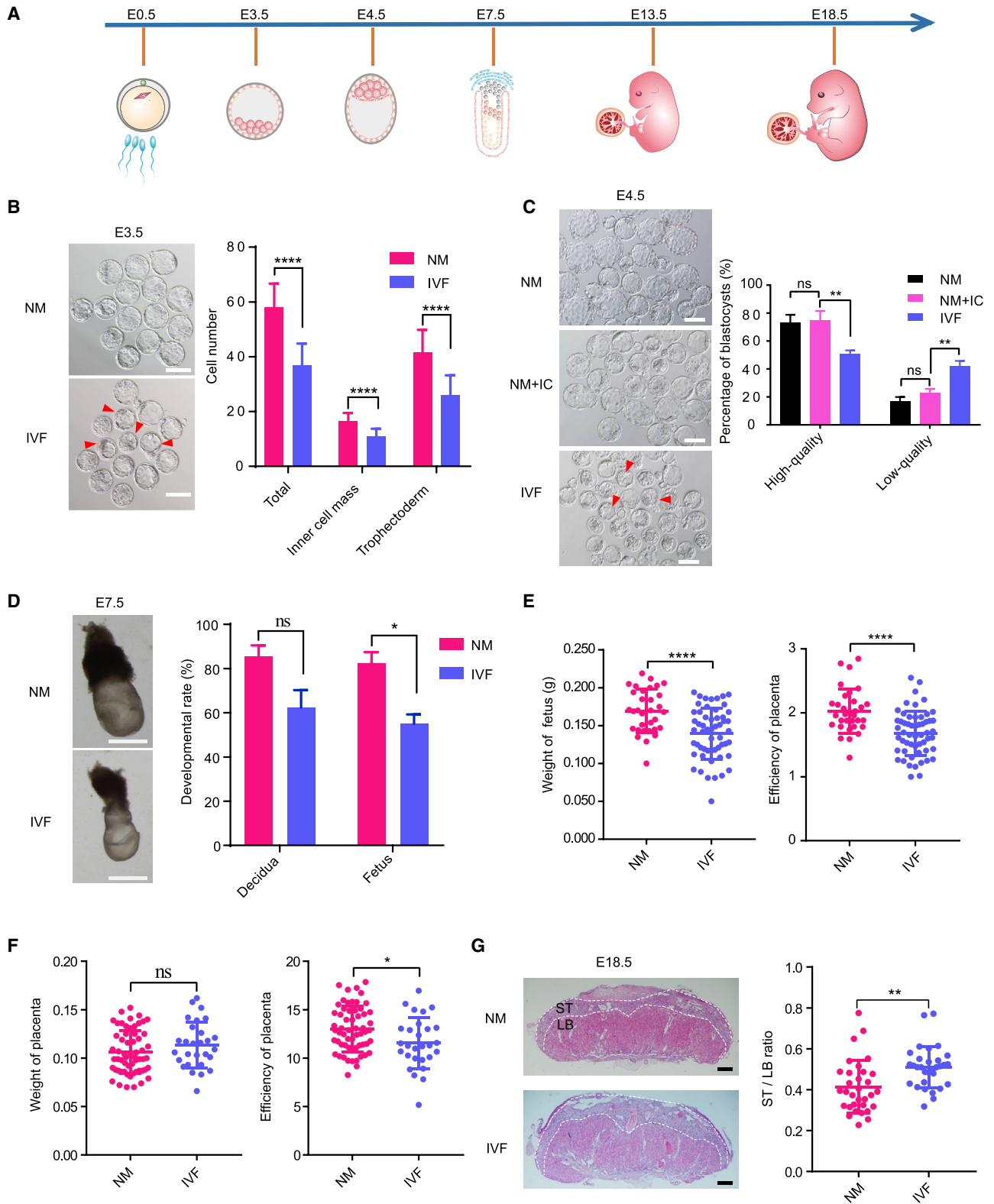
(legend on next page)

Vastenhouw and Schier, 2012; Xiang et al., 2020). Moreover, H3K27me3 located in promoters maintains noncanonical imprinting before implantation and is replaced by DNA methylation in the extraembryonic ectoderm (ExE) after implantation (Hanna et al., 2019; Inoue et al., 2017). Abnormal and incomplete establishment of epigenetic modifications in extraembryonic tissues is one of the reasons leading to fetal nutritional restriction and death. Studies have shown that abnormal and insufficient DNA methylation establishment in decidual tissue of placenta can lead to an increased abortion rate (Brown et al., 2013; Yin et al., 2012). Abnormal establishment of DNA methylation and expression of imprinting genes lead to embryo death due to defective placental function (Arima et al., 2006; Tunster et al., 2016). Placental defects promote embryonic complications in IVF embryos. Studies on DNA methylation of IVF placentas have found that hypomethylation of the imprinting control region (ICR) promotes the expression of imprinting genes (de Waal et al., 2014, 2015). Previous research mainly focused on DNA methylation at specific sites, imprinted gene regulation, and noncoding RNA (Apicella et al., 2019; de Waal et al., 2015; Duranthon and Chavatte-Palmer, 2018). Genome-wide histone modification profiling during the implantation process could reveal the relationships between histone modifications and IVF embryo abnormalities.

Here, we explored the effects of IVF on mouse embryo development, gene expression, and histone modification. High ectopic expression of epiblast (Epi)-specific genes in extraembryonic tissues led to abnormal cell lineage establishment, which influenced the development of the extraembryonic tissues of IVF embryos. Disruption of H3K4me3 modifications in the promoter regions of genes and abnormal widening in the transcription factor region led to ectopic expression of Epi genes in IVF extraembryonic tissues, which may be an important cause of abnormal development of IVF embryo extraembryonic tissues. Interfering with the H3K4me3-modified gene *Kmt2e* improved the development of IVF embryos and rescued ectopic gene expression in extraembryonic tissues. Our research identifies that abnormal accumulation of H3K4me3 in extraembryonic tissues is one of important reasons for the abnormal development of IVF embryos

and provides a promising approach for improving the success rate of IVF.

RESULTS

Defects in embryonic and extraembryonic developmental trajectories in IVF embryos

To systematically evaluate the effects of IVF on both embryonic and extraembryonic tissue, we established an IVF model to track the development from preimplantation to intrauterine period. BDF1 (C57BL/6N female × DBA2 male) mice were used to obtain embryos (embryos derived from *in vitro* fertilization and *in vitro* culture were defined as IVF embryos, embryos derived from natural mating and *in vivo* development were defined as NM embryos, and embryos derived from natural mating and *in vitro* culture were defined as NM + IC embryos). We first evaluated the effects of IVF on the development of early embryos, fetuses, and placentas at embryonic day 3.5 (E3.5), E4.5, E7.5, E13.5, and E18.5 (Figure 1A). We found that embryo loss occurred mainly in the early stage of implantation (Figure S1A).

Similar to the findings in previous reports, the blastocyst rate of IVF embryos was over 90% (Figure S1B) (Movahed et al., 2020; Shinar, 2018). However, compared with NM blastocysts, IVF blastocysts showed dilation defects at E3.5, and the total cell number was significantly lower for IVF blastocysts than for NM blastocysts (IVF 36.82 versus NM 58.04) (Figure 1B). Furthermore, the difference in cell number between the two groups was caused mainly by the large reduction in TE cells (IVF 25.91 versus NM 41.58) (Figure 1B). Dilatation and hatching from the zona pellucida at the late blastocyst stage (E4.5) are required for implantation and intrauterine growth. We also found that the proportion of high-quality blastocysts (undergoing both dilatation and hatching) in the IVF group was 50.65%, which was much lower than that in the NM + IC group (74.53%) and NM group (72.96%) (Figure 1C). Moreover, the percentage of low-quality (undergoing only dilatation or hatching) blastocysts in the IVF group was much higher than that in the control group (IVF 41.84% versus NM + IC 22.74% versus NM 16.51%) (Figure 1C).

Figure 1. Defects in embryonic and extraembryonic developmental trajectories in IVF embryos

(A) Schematic representation of embryonic development at E3.5, E4.5, E7.5, E13.5, and E18.5.

(B) The development and cell numbers of E3.5 blastocysts of IVF and NM embryos. The red arrows (left) denote low-quality blastocysts. The ICM and the TE (right) were identified separately with anti-NONOG and anti-CDX2 antibodies. The cell number was counted with ImageJ, and the supporting data are shown in Table S2. Scale bar, 100 μm. The data are presented as the mean ± SD (numbers of total, TE and ICM cells analyzed: n = 22 for IVF, n = 24 for NM). Unpaired Student's t test, ****p < 0.0001.

(C) Embryonic development of the IVF, NM, and NM + IC groups at the E4.5 blastocyst stage. NM represents embryos obtained *in vivo* at E3.5 and cultured until hatching at E4.5. NM + IC represents embryos obtained *in vivo* at the zygote stage and cultured until hatching at E4.5. High-quality blastocysts refer to embryos with dilatation and hatching. Low-quality blastocysts refer to embryos with only dilatation or hatching. The red arrows (left) denote low-quality blastocysts. Scale bar, 100 μm. The data are presented as the mean ± SD, and the supporting data are shown in Table S1 (for analysis of the percentages of high-quality blastocysts and low-quality blastocysts: n = 3 for IVF, NM, and NM + IC). Unpaired Student's t test, **p < 0.01.

(D) Embryonic development of the IVF and NM groups at E7.5. Scale bar, 500 μm. The data are presented as the mean ± SD, and the supporting data are shown in Table S1 (for analysis of the developmental rate of the decidua and fetus: n = 2 for IVF and NM). Unpaired Student's t test, *p < 0.05.

(E) Embryonic and placental development of the IVF and NM groups at E13.5. The placental efficiency is the fetal weight/placental weight, and the supporting data are shown in Table S3. The data are presented as the mean ± SD (n = 55 for IVF, n = 32 for NM). Unpaired Student's t test, ****p < 0.0001.

(F) Placental weight and efficiency of IVF embryos and NM embryos at E18.5. The supporting data are shown in Table S3. The data are presented as the mean ± SD (for analysis of the placental weight and efficiency: n = 28 for IVF, n = 59 for NM). Unpaired Student's t test, *p < 0.05.

(G) Placental development of the NM and IVF groups at E18.5. Scale bar, 500 μm. The spongiotrophoblast layer (ST)/labyrinth layer (LB) ratio was used to evaluate the quality of the placenta. The areas of ST and LB were counted with ImageJ. The data are presented as the mean ± SD, and the supporting data are shown in Table S4 (n = 31 for IVF, n = 32 for NM). Unpaired Student's t test, **p < 0.01.
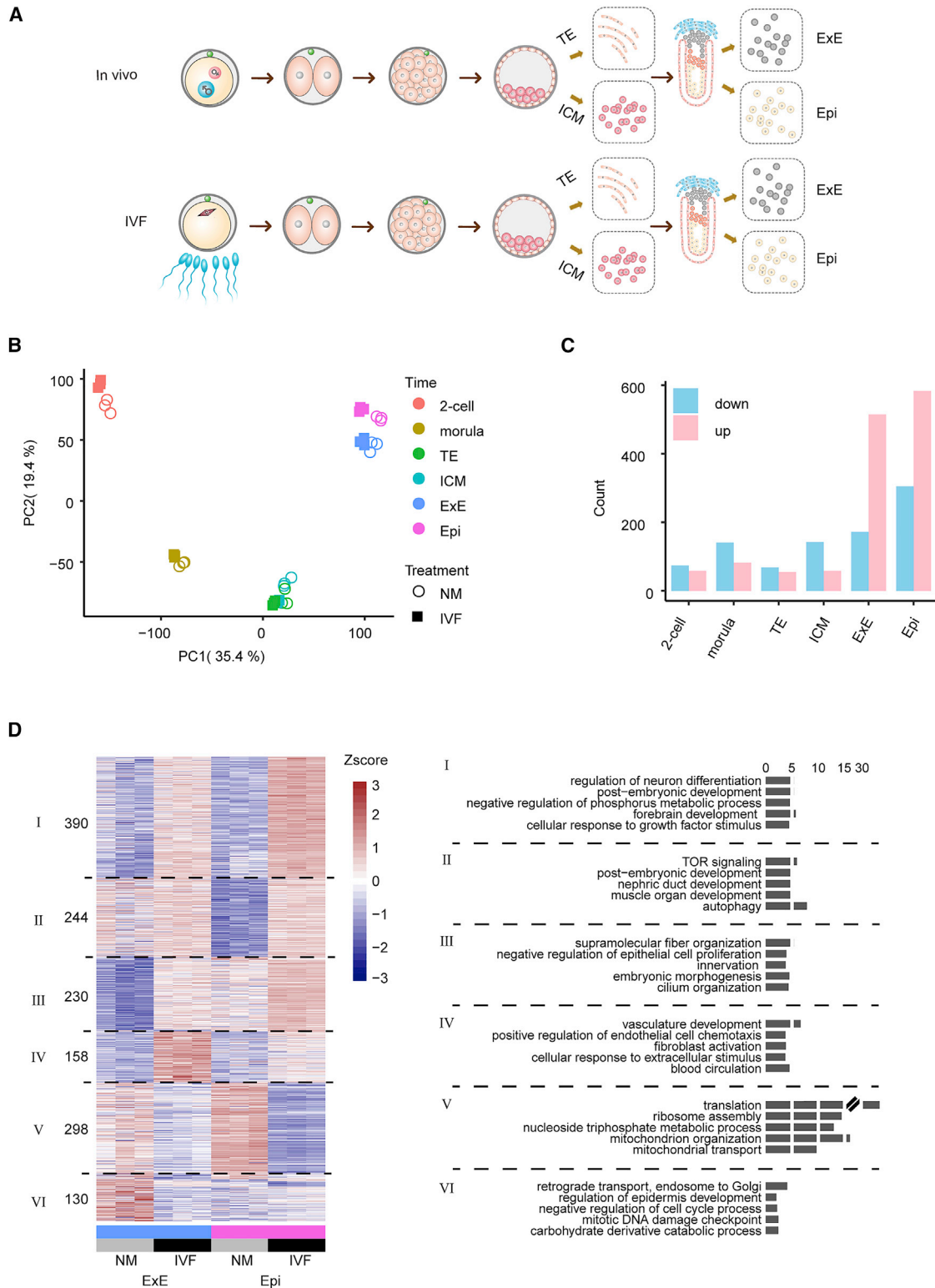
Figure 2. Abnormal gene expression in embryonic and extraembryonic tissues of IVF embryos

(A) Schematic representation of the RNA-seq transcriptomic data from IVF embryos and NM embryos at the two-cell, morula, E3.5 blastocyst (TE, ICM), and E7.5 (Epi, ExE) stages.

These results indicate that IVF may influence blastocyst quality and developmental potential.

Embryo loss occurred mainly at approximately E7.5, a time point that is also crucial for subsequent development of the embryo and placenta. We established that the number of deciduas and embryos in IVF group was significantly lower than in NM group at E7.5 (Figure 1D), and the embryo size in the IVF group was significantly smaller than in the NM group at E7.5 (Figure S1C). Although IVF embryos grew until E13.5 and E18.5, placental abnormalities significantly affected fetal growth (Figures 1E, S1D, S1E, and S1F). Analysis of placental efficiency (fetal weight/placental weight) (Hayward et al., 2016), a common way to evaluate placental function in both humans and animals, revealed that IVF embryos were significantly less efficient than NM embryos at both E13.5 and E18.5 (Figures 1E and 1F). Analysis of placental slices at E18.5 showed that the IVF placenta was characterized by a significantly thickened spongiotrophoblast layer, thinned labyrinth layer, and increased ratio of spongiotrophoblast to labyrinth layer (Figures 1G and S1G). This suggests that the developmental defects of extraembryonic tissue continue throughout the embryonic development period.

Abnormal gene expression in embryonic and extraembryonic tissues of IVF embryos

To identify the effect of IVF on gene expression, we performed RNA sequencing (RNA-seq) of NM and IVF embryos at the two-cell, morula, E3.5 blastocyst (TE; Inner cell mass, ICM), and E7.5 stages (Epi, ExE) via single-cell RNA-seq method (Figure 2A) (Tang et al., 2009, 2010). Cluster analysis revealed that the gene expression pattern of IVF embryos was similar to that of NM embryos (Figure 2B). This was consistent with the fact that most IVF embryos can develop normally and produce relatively normal fetuses (Figures S1E and S1F). Furthermore, we identified 132, 223, 123, 200, 687, and 888 differentially expressed genes in two-cell, morula, E3.5 TE, E3.5 ICM, E7.5 ExE, and E7.5 Epi between the IVF group and NM group with stringent cutoffs (DESeq2 fold change >4 and p.adj <0.01) (Figure 2C). Gene Ontology analysis revealed that the differentially expressed genes were enriched in the processes of mitochondrial function, RNA transcription, embryonic morphogenesis, and cardiovascular and nervous systems, indicating that IVF embryos have gene expression disorders (Figure S2A). As a large number of differentially expressed genes were observed at the E7.5 stage in IVF embryos, we divided the differentially expressed genes into six groups: genes upregulated in both Epi and ExE (group I), genes upregulated in Epi (group II), genes upregulated in ExE (groups III and IV), genes downregulated in Epi (group V), and genes downregulated in ExE (group VI) (Figure 2D). Strikingly, the genes of groups III and IV were enriched for innervation, embryonic morphogenesis, vasculature devel-

opment, blood circulation, and other functions that are highly related to embryonic development, showing the disruption of IVF ExE gene expression (Figure 2D). Imprinted genes are very important for the development of embryonic and extraembryonic tissues, and abnormal expression has been reported in IVF embryos (Cleaton et al., 2014; Eroglu and Layman, 2012; Fowden et al., 2011; Smith et al., 2006). We discovered that 17 imprinted genes were differentially expressed in at least one stage between IVF embryos and NM embryos (DESeq2 fold change >4 and p.adj <0.01) from the two-cell stage to the E7.5 stage (Figure S2B). Overall, slight downregulation of imprinted genes was observed in IVF embryos before implantation (Figure S2B). In contrast, drastic upregulation of imprinted genes emerged in IVF embryos after implantation (Figure S2B). These results indicate that with development, the gene expression of IVF embryos showed increasing transcriptomic disruption, and the differentially expressed genes of IVF embryos were correlated with embryonic developmental defects.

Impaired lineage establishment of extraembryonic tissue after IVF implantation

After implantation, the TE and ICM of the blastocyst transform into ExE and Epi, respectively, which have different lineage identities, cell morphologies, and transcriptomes. To reveal the effect of IVF on lineage differentiation of ExE and Epi, we defined 1,114 lineage-specific genes that were differentially expressed genes (DESeq2 fold change >4 and p.adj <0.01) between ExE and Epi in NM embryos, including 709 Epi-specific genes and 405 ExE-specific genes (Figure 3A). By comparing the gene expression of NM and IVF embryos, we identified 334 Epi-specific genes that were ectopically expressed in the ExE of IVF embryos (Figure 3A). This implied that the lineage identity of extraembryonic tissues in IVF embryos was disturbed.

Cell type-specific transcription factors (TFs) play essential roles in cell fate determination by controlling tissue-specific gene expression. We further defined 36 Epi-specific TFs (DESeq2 fold change >4 and p.adj <0.01 between ExE and Epi, expression: log2CPM >3 in Epi and log2CPM <2 in ExE) and 40 ExE-specific TFs (DESeq2 fold change >4 and p.adj <0.01 between ExE and Epi, expression: log2CPM >3 in ExE and log2CPM <2 in Epi) in NM embryos (Figure 3B). Similar to the lineage-specific genes, 26 Epi-specific TFs in the ExE of the IVF embryos were upregulated more than 2-fold, while NM and IVF embryos featured nearly unchanged expression of ExE-specific TFs (Figure 3B). To further reveal whether ectopic expression is related to these transcription factors, we analyzed *Oct4* (an Epi-specific TF that is overexpressed in ExE of IVF embryos) target genes and revealed that they were enriched among the upregulated genes, suggesting that disruption of TF expression may aggravate abnormal differentiation in the ExE lineage of IVF embryos (Figure 3C). Our results

(B) Principal-component analysis showing the gene expression profiles in IVF embryos and NM embryos. The color indicates the developmental stage, and the shape indicates the sample type.

(C) Numbers of differentially expressed genes between IVF embryos and NM embryos at different developmental stages. The differentially expressed genes satisfied stringent cutoffs (DESeq2 fold change >4 and p.adj <0.01).

(D) Heatmap showing the differentially expressed genes (total number: 1,450) in (C) of Epi and ExE, which were classified into six groups. The Gene Ontology analysis results for these six groups are shown on the right.

A

B

C
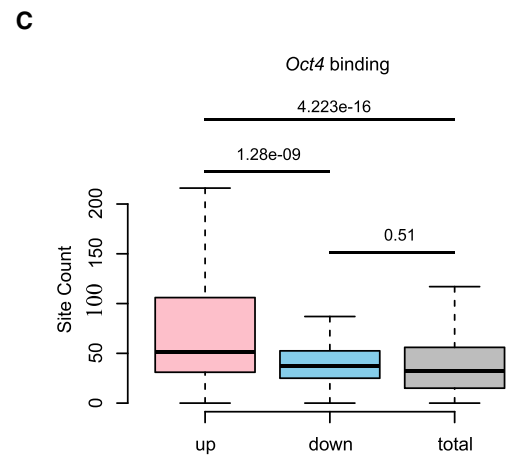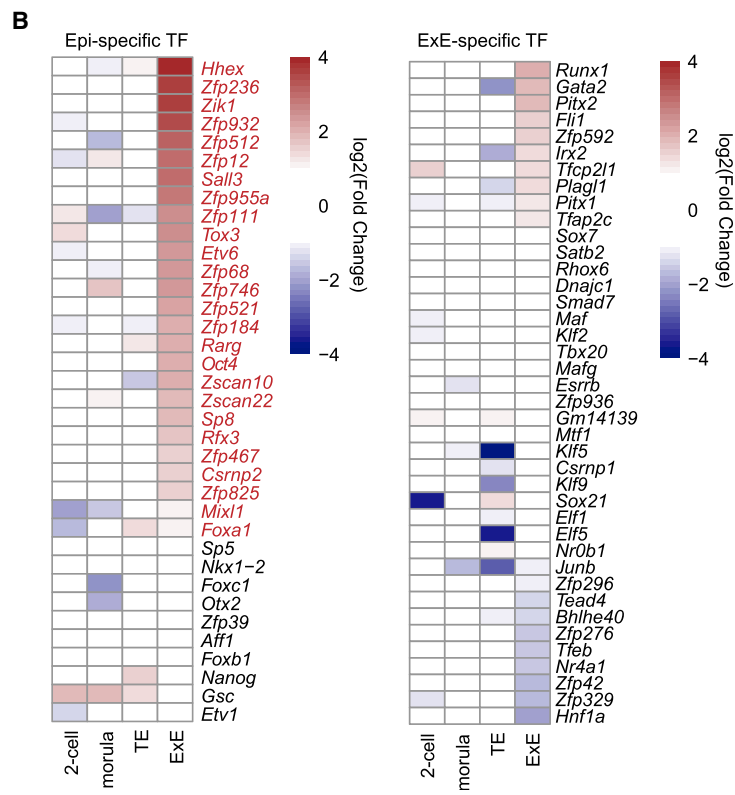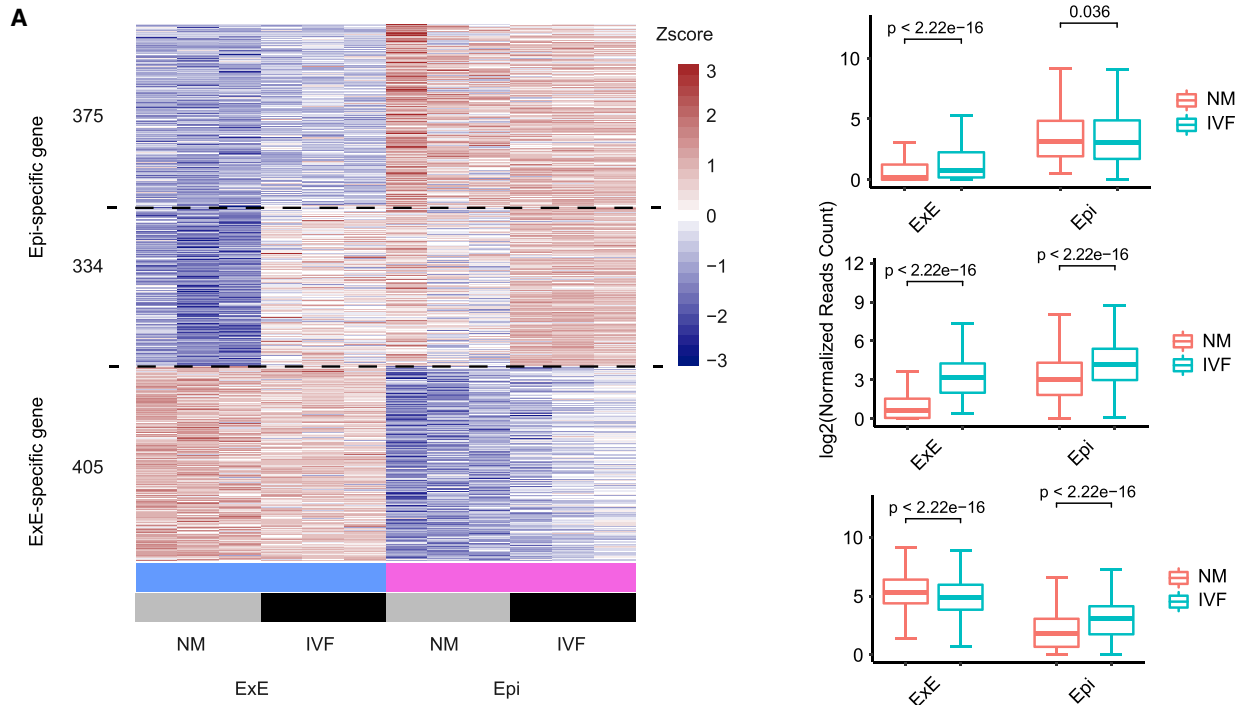
(legend on next page)

proved that ExE lineage differentiation of IVF embryos was disrupted.

Identification of anomalous H3K4me3 modification in ExE of IVF embryos

Early embryonic development is accompanied by dramatic epigenetic reprogramming and chromatin remodeling processes. Histone modifications play critical roles in gene expression and cell lineage differentiation, and genes with H3K4me3 or H3K4me3/H3K27me3 bivalents are associated with transcriptional activation, where H3K27me3 modifications are thought to be positioned for silencing (Iwagawa and Watanabe, 2019; Liu et al., 2016, 2019; Meng et al., 2019). The remodeling of broad H3K4me3 and H3K4me3/H3K27me3 bivalent patterns is closely related to embryonic development and tissue specificity establishment (Dahl et al., 2016; Liu et al., 2016; Zhang et al., 2016). To precisely dissect the histone changes of IVF embryos, we generated H3K4me3 and H3K27me3 landscapes of morulae, E3.5 blastocysts (TE, ICM), and E7.5 embryos (ExE, Epi) from the IVF and NM groups via ultra-low-input micrococcal nuclease-based native chromatin immunoprecipitation (ULI-NChIP) (Brind'Amour et al., 2015; Liu et al., 2016).

Genome-wide analysis of these two modifications revealed that the distribution was consistent between IVF and NM embryos (Figure S3A). ChromHMM analysis (in which the histone modification state was defined as H3K4me3-only state, H3K27me3-only state, bivalent state, or unmarked state) showed that IVF and NM embryos had similar histone modification states, especially the bivalent state (Figure 4A, 4B, and S3B) (Ernst and Kellis, 2012; Liu et al., 2016). Nevertheless, a differential histone modification state still existed in the IVF group pre- and post-implantation, especially demonstrated increased H3K4me3 modification in TE (Figure 4C). To further study the influence of IVF on the distribution of histone modifications, we strictly defined the major differentially modified regions (the top 5% differential regions) between IVF embryos and NM embryos as those that satisfied both the chromatin state change and histone modification difference and performed a cluster analysis (Figure 4D). Unexpectedly, the major differentially modified regions in the ExE of IVF embryos were more similar to the Epi of NM embryos than to the ExE of NM embryos (Figure 4D). Further analysis revealed that the abnormal location of H3K4me3 modification instead of H3K27me3 modification in ExE must have been responsible for the similarity to Epi (Figures 4E and S3C). In addition, accumulation of ectopic H3K4me3 modifications in the transcription start site (TSS) and the promoters promoted gene expression (Figures 4F and S3D). These results proved that IVF manipulation affects histone modification-related remodeling of early post-implantation embryos, especially in extraembryonic tissues.

Aberrant H3K4me3 modification is associated with the activation of Epi lineage genes in IVF ExE tissue

Based on the combinations of histone modification state characteristics, we defined 124 Epi active promoters (with occupancy of H3K4me3 active histone marks in Epi but not in ExE) and 85 ExE active promoters (with occupancy of H3K4me3 active histone marks in ExE but not in Epi) (Figures 5A and S4A). Notably, the Epi active promoter region was ectopically enriched with H3K4me3 marks in IVF ExE tissues, while the ExE active promoter region was comparable between NM and IVF ExE tissues (Figures 5A, 5B, and S4A). Further transcriptome analysis revealed that 93 of 124 Epi active promoter marked genes were upregulated in IVF ExE compared with NM embryos; these genes were defined as ectopic H3K4me3-marked genes (Figure 5C). Gene Ontology analysis revealed that the main functions of these genes were anterior and posterior specification, cell fate specification, and stem cell differentiation, which play important roles in the specialization of embryonic development rather than in extraembryonic tissues (Figure 5C).

Previous studies have also shown that the width of H3K4me3 affects not only gene expression but also tissue specificity (Benayoun et al., 2014; Park et al., 2020). To verify the effect of H3K4me3 modification width on gene expression, we analyzed the differentially expressed genes occupied by H3K4me3 in IVF embryos; 410 upregulated genes showed widened H3K4me3 areas in the ExE of IVF embryos, but not 138 downregulated genes (Figure S4B). Furthermore, 334 upregulated Epi-specific genes were occupied by H3K4me3 in a wider area in IVF ExE than in NM ExE (Figure 5D). We next analyzed the H3K4me3 modification widths of 36 Epi-specific TFs. Eight of 36 Epi-specific TFs showed abnormally broad H3K4me3 signals (>10 kb) in the ExE tissue of IVF embryos, which was a feature of NM Epi (Figure 5E). Furthermore, 16 Epi-specific TFs showed wider H3K4me3 ($\geq$1 kb) in IVF ExE than in NM ExE, and the gene expression was significantly higher in the IVF ExE than in the NM ExE (Figure 5F). Collectively, our research showed that ectopic H3K4me3 modification was associated with abnormal gene expression in the extraembryonic tissues of IVF embryos.

Abnormal accumulation of H3K4me3 modification influenced the development of extraembryonic tissues in NM embryos

To further investigate the relationship between abnormal accumulation of H3K4me3 modification and abnormal embryo development, we injected *Kdm5b* small interfering RNA (siRNA), which is an H3K4me3 eraser, at the zygote (PN3-PN4) stage of NM embryos and then assessed embryonic development at E3.5, E4.5, E7.5, E13.5, and E18.5. The NM embryos injected with *Kdm5b* siRNA were defined as the *siKdm5b* group, and

---

Figure 3. Impaired lineage establishment of extraembryonic tissue after IVF implantation

(A) Expression of Epi-specific genes and ExE-specific genes in IVF embryos and NM embryos. Lineage-specific genes were defined between Epi and ExE of the NM group with stringent cutoffs (fold change >4 and p.adj <0.01) using DESeq2. Genes with a maximum expression >2 (normalized read count >3) and genes with large variance among biological replicates were discarded.

(B) Expression of Epi-specific TFs and ExE-specific TFs in IVF embryos. The Epi-specific TFs and ExE-specific TFs were subsets of those in Figure 3A. The expression of Epi-specific TFs satisfied log2CPM >3 in Epi and log2CPM <2 in ExE; the expression of ExE-specific TFs satisfied log2CPM >3 in ExE and log2CPM <2 in Epi. Epi-specific TFs upregulated in IVF ExE are highlighted in red.

(C) Numbers of *Oct4* binding sites among the upregulated genes, downregulated genes, and total genes in ExE of IVF embryos.
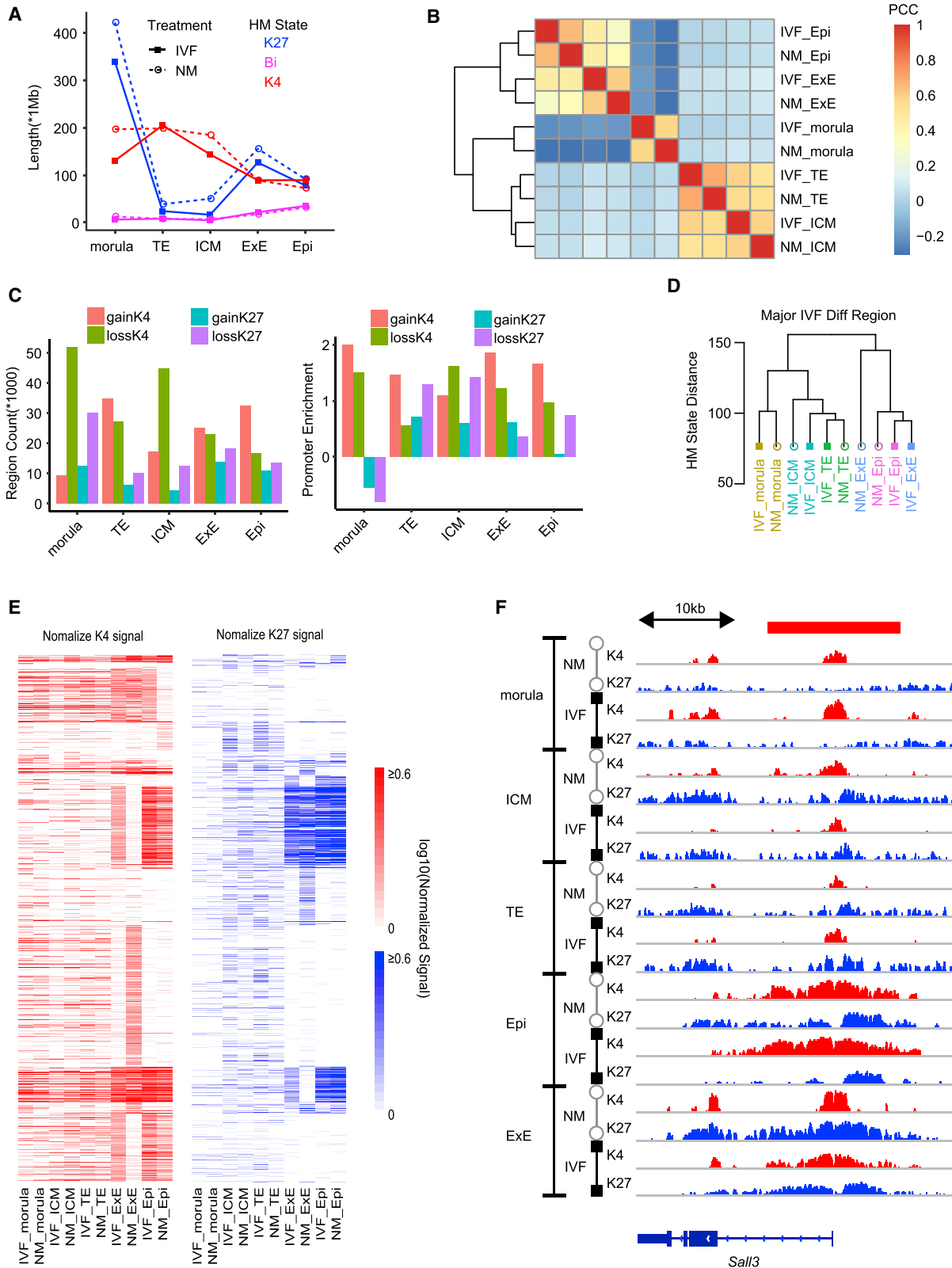
(legend on next page)

the NM embryos injected with water were defined as the NM control group. The knockdown efficiency of *Kdm5b* was evaluated at the E3.5 blastocyst stage (Figure S5A). Knockdown of Kdm5b in NM embryos not only affected the cell number of TE at E3.5 but also influenced the quality of E4.5 embryos (Figures S5B and S5C). Meanwhile, the implantation and development declined in the *siKdm5b* group compared with that in the NM control group (Figure S5D). To explore whether *Kdm5b* could influence the gene expression in extraembryonic tissue, we performed E7.5 ExE transcriptome analysis of NM control and *siKdm5b* embryos via the Smartseq2 RNA-seq method (Picelli et al., 2014). *Kdm5b* knockdown resulted in 307 upregulated genes and 63 downregulated genes in ExE compared with that of NM control group (DESeq2 fold change >2 and p.adj <0.05) (Figure S5E). Gene Ontology analysis revealed that those upregulated genes were mainly enriched in embryonic morphogenesis and embryonic development, which was similar to IVF embryos (Figure S5F). In addition, promoters of upregulated genes in the *siKdm5b* group showed increased H3K4me3 modification (Figure S5G), indicating that the abnormal accumulation of H3K4me3 modification caused by *Kdm5b* knockdown leads to ectopic expression of embryonic genes in ExE. In the middle stage of embryonic development (E13.5), fetal developmental speed and placental efficiency were significantly decreased after *Kdm5b* siRNA injection (Figure S6A). More importantly, the fetal survival rate at the final stage of intrauterine development (E18.5) significantly declined in the *siKdm5b* group (Figure S6B). Notably, the placental weight of the *siKdm5b* group was significantly increased, while the placental efficiency was not affected (Figure S6C). Further evaluation of placental structure revealed that the proportion of the placental spongiotrophoblast layer increased significantly by *Kdm5b* interference, while the proportion of the labyrinth layer decreased significantly, which was similar to IVF embryos (Figure S6D). Those results suggest that abnormal accumulation of the H3K4me3 modification can affect the embryonic and extraembryonic development.

Knockdown of *Kmt2e* expression restores the development of IVF extraembryonic tissue

Having established a correlation between ectopic H3K4me3 modification and abnormal gene expression in extraembryonic tissues, we next analyzed the expression of H3K4me histone modification enzymes, including writers, readers, and erasers (Figure S7A). A heatmap of gene expression showed that *Kmt2e* was abnormally highly expressed in two-cell and E7.5 embryos (Figure S7A). Previous studies have shown that *Kmt2e* expression is accompanied by elevated levels of H3K4me3-modified gene expression (Sebastian et al., 2009). We next investigated whether knocking down *Kmt2e* could

restore the development of IVF embryos. We injected *Kmt2e* siRNA at the zygote (PN3-PN4) stage and then evaluated embryonic development at E3.5, E4.5, E7.5, E13.5, and E18.5 in IVF embryos. IVF embryos injected with *Kmt2e* siRNA were defined as the *siKmt2e* group, IVF embryos injected with water were defined as the IVF control group, and *in vivo* fertilized zygotes injected with water were defined as the NM control group. The knockdown efficiency of *Kmt2e* was evaluated at the E3.5 blastocyst stage (Figure S7B). Surprisingly, the blastocyst rate (E3.5) in the *siKmt2e* group was similar to that of the NM control group (Figure S7C). Strikingly, knockdown of *Kmt2e* not only significantly improved the quality of blastocysts but also increased the number of embryos implanted (E7.5) (Figures 6A, 6B, 6C, and S7D). In the middle stage of embryonic development (E13.5), fetal development speed and placental efficiency were significantly improved after *Kmt2e* siRNA injection (Figures 6D and S7E). More importantly, the fetal survival rate at the final stage of intrauterine development (E18.5) was increased significantly in the *Kmt2e* intervention group, which was consistent with the survival rate increase of the E7.5 fetuses (Figures 6C and S7F). Notably, the placental weight in the *siKmt2e* group was significantly reduced, while the placental efficiency was significantly improved, similar to the case in the NM control group (Figures 6E and S7G). Further evaluation of the placental structure revealed that the proportion of the placental spongiotrophoblast layer decreased significantly after interference, while the proportion of the labyrinth layer increased significantly (Figures 6F and S7H). Furthermore, the *siKmt2e* group had an increased birth rate, and postnatal growth was not affected (Figures S7I and S7J). Our results indicated that early interference with *Kmt2e* can rescue the development of IVF extraembryonic tissue and further promote embryonic development.

Kmt2e interference ameliorates the changes in lineage-specific gene expression in IVF ExE tissue

We next investigated the molecular mechanisms that could be responsible for restoring IVF extraembryonic tissue development. To explore whether interference with *Kmt2e* could ameliorate the changes in extraembryonic tissue gene expression of IVF embryos, we first analyzed E7.5 ExE transcriptome data of IVF control and *siKmt2e* embryos performed by Smartseq2 RNA-seq method (Picelli et al., 2014). Clustering revealed that the gene expression of IVF embryos with *Kmt2e* knockdown was corrected and similar to that of NM embryos (Figure 7A). *Kmt2e* knockdown significantly decreased the expression of 93 ectopic H3K4me3-marked genes (Figure 7B). Moreover, the expression of 334 upregulated Epi-specific genes was decreased in ExE after *Kmt2e* knockdown (Figure 7C). The expression of 36 Epi-specific TFs was decreased after *Kmt2e*

Figure 4. Identification of anomalous H3K4me3 modification in ExE of IVF embryos

(A) Distribution and variation of histone modification states in the genome. The histone modification state was defined as an H3K4me3-only state, an H3K27me3-only state, a bivalent state, and an unmarked state using ChromHMM analysis at a length of 1 Mb.

(B) Heatmap showing the cluster of histone modification states between NM and IVF embryos.

(C) Number of differential histone modifications in the defined histone modification state regions of IVF embryos.

(D) Cluster analysis of differential histone modification states between NM embryos and IVF embryos.

(E) Heatmap showing the differential histone modifications of H3K4me3 and H3K27me3 in (D).

(F) Genome browser view of the differential histone modification state distribution on *Sall3*. The red box indicates the differential histone modification state.

A

Epi Active Promoter(124)

B

ExE

C

ExE(93)
P=9e−5

D

334 Epi-specific genes

E

F

ExE(16)
P=5e−4
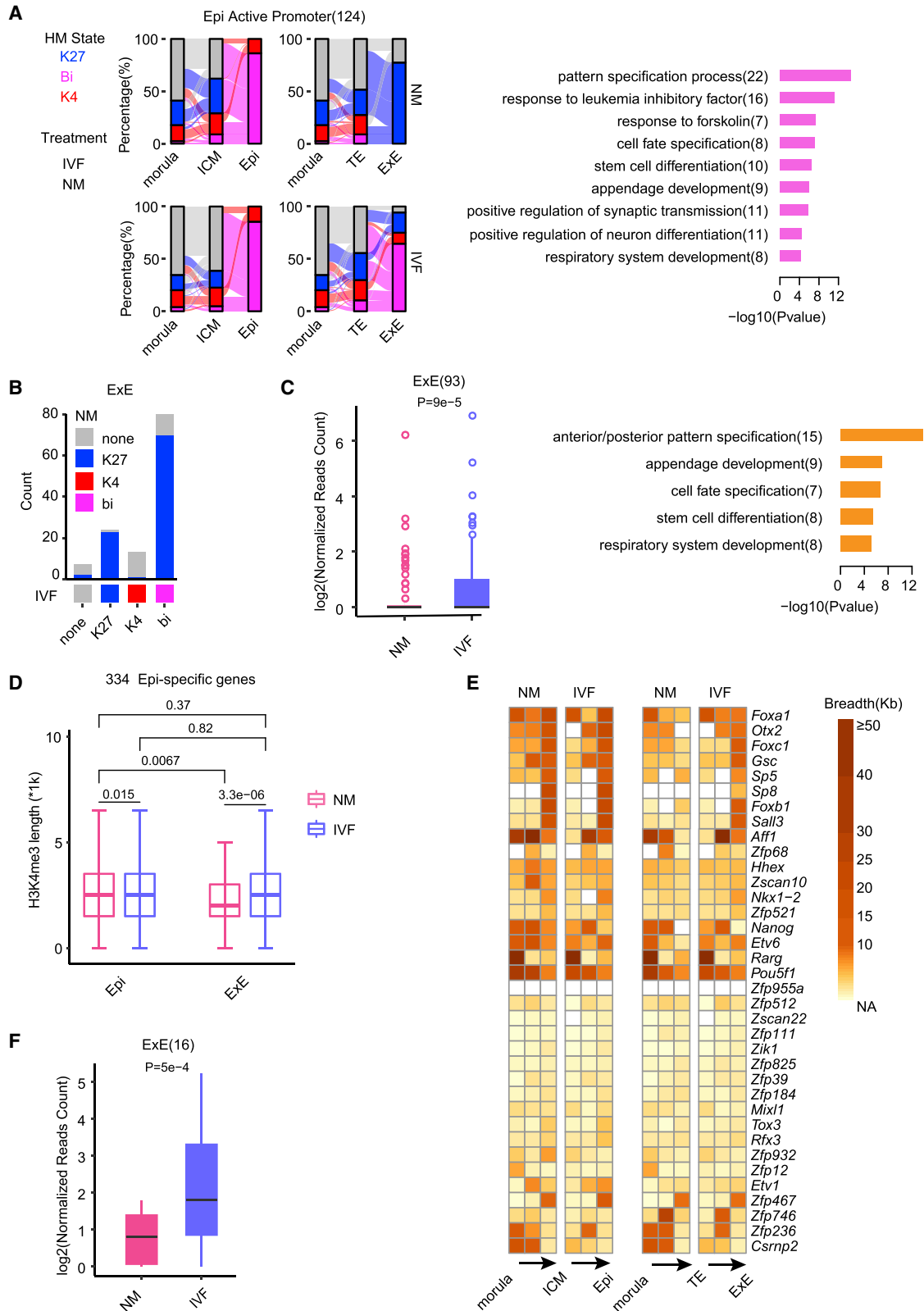
(legend on next page)

knockdown to the levels similar to those in NM embryos (Figures 7D and 7E). This suggested that modification of the expression of *Kmt2e* improved IVF extraembryonic tissue identity. We further explored the relationship between *Kmt2e* and H3K4me3 modifications with regard to gene expression, and we found that there were 410 upregulated genes with H3K4me3 occupancy in the ExE of IVF embryos and 48 upregulated genes without H3K4me3 occupancy. After we interfered with the expression of *Kmt2e*, genes with the H3K4me3 occupancy were obviously rescued, but the genes without H3K4me3 occupancy were not obviously changed in *siKmt2e* E7.5 ExE (Figure 7F). These results showed that *Kmt2e* promoted gene expression depending on the presence of H3K4me3 modification.

DISCUSSION

Despite the remarkable improvements in the past decade, IVF is still associated with reduced pregnancy rates and elevated miscarriage rates (Bu et al., 2020; Zeadna et al., 2015). Moreover, reduced placental efficiency, placental overgrowth, and low birth weight have also been observed in humans and animals, indicating that IVF might have adverse effects on embryonic development (Bloise et al., 2012; de Waal et al., 2015; Fauser et al., 2014; Jauniaux et al., 2020; von Wolff and Haaf, 2020). By tracing the development of embryos, we found that IVF embryos showed more severe abnormalities in extraembryonic tissue development than NM embryos, including decreased numbers of TE cells, which led to disturbances in the structure and function of the placenta after implantation. This is consistent with previous reports in humans and animals (de Waal et al., 2015; Shinar, 2018). These results suggest that extraembryonic tissue is more sensitive than embryonic tissue to IVF treatment. Furthermore, defects of the placenta are important factors leading to abnormal IVF embryonic development and long-term health problems in offspring. These abnormalities may be related to changes in epigenetic modifications resulting from IVF procedures. The mechanism leading to abnormal embryonic development needs to be further explored.

Epigenetic modification is a key determinant of important developmental events in embryo implantation, cell lineage differentiation, and placental development. H3K4me3 and H3K27me3 modification plays a significant role in the regulation of key developmental genes. A recent study reported that Epi-specific developmental genes are regulated by H3K27me3 and are silenced by DNA methylation in ExE tissues, which is believed to be conducive to maintaining the highly regulated developmental plasticity of embryonic cells and permanently limiting the developmental potential of ExE (Yang et al., 2018). Our previous study has also

shown that the breadth of H3K4me3 modification is essential for the differentiation of TE and ICM (Liu et al., 2016). We revealed that although H3K4me3 modification remained stable during the development of TE to ExE, upregulation of IVF-related gene and TF expression was significantly associated with increased breadth of H3K4me3 modification. This highlights the importance of H3K4me3 breadth regulation in developmental gene expression. We identified an ectopic increase of H3K4me3 in IVF ExE tissue. The ectopic H3K4me3 levels were significantly correlated with ectopic expression of embryonic development genes. These results suggest a potential role for H3K4me3 levels in embryo implantation failure and subsequent placental dysplasia.

The analysis of H3K4me3 modification-related genes revealed that *Kmt2e* was highly expressed at the two-cell stage and subsequently highly expressed in the extraembryonic tissues of IVF embryos. As a member of the mixed lineage leukemia (MLL) family, *Kmt2e* has a single suppressor of variegation, enhancer of zeste, trithorax (Set) domain, and a single plant homeodomain (PHD), which is highly conserved among species and functions as a reader, rather than a writer, of H3K4me3 (Ali et al., 2013; Madan et al., 2009; Sebastian et al., 2009; Zhang et al., 2017). Our data show that knockdown of *Kmt2e* can correct abnormal expression only of genes with H3K4me3 occupancy. This suggests that *Kmt2e* promotes gene expression depending on H3K4me3 modification in IVF embryos. However, whether the increase in *Kmt2e* expression selectively enriches H3K4me3-modified genes and whether TFs are recruited for comprehensive regulation requires further research. Although we did not evaluate the long-term risk of interfering with *Kmt2e* in mice after birth, our study provides new mechanistic and clinical insights to improve the developmental potential of IVF embryos.

In addition, IVF embryos also exhibited abnormalities in embryonic tissue pre- and post-implantation, including reducing the cell number of inner cell mass at the blastocyst stage, existing differentially expressed genes, and histone modification. Differentially expressed gene analysis found that the upregulated genes of IVF Epi (group II) were enriched in TOR and autophagy-related pathways, which may be an important way that IVF embryos respond to environmental stress to enhance implantation and post-implantation development. Autophagy is an effective way to cope with the stress of embryonic survival. Increased autophagy may contribute to embryonic development, including cloned embryo quality, *in vitro* preimplantation embryo development, and implantation (Bai et al., 2019; Lee et al., 2016; Shen et al., 2015). In addition, the downregulated genes of IVF Epi (group V) were enriched in the processes of translation, ribosomal and mitochondrial function, and nucleoside triphosphate metabolism, which may be related to the retarded development of IVF embryos. Embryonic tissue

---

Figure 5. Aberrant H3K4me3 modification is associated with the activation of Epi lineage genes in IVF ExE tissue

(A) Histone modification state and Gene Ontology (GO) analysis of Epi active promoters. Epi active promoters were defined in NM embryos as those with occupancy of the active histone mark H3K4me3 in Epi but not in ExE.

(B) Variations of Epi active promoters in IVF ExE.

(C) Gene expression and GO analyses of 93 genes marked with Epi active promoters in IVF ExE.

(D) H3K4me3 modification widths of 334 upregulated Epi-specific genes.

(E) H3K4me3 modification widths of 36 Epi-specific TFs in IVF ExE.

(F) Expression of 16 Epi-specific TFs with relatively wide H3K4me3 regions (≥1 kb) in IVF ExE.
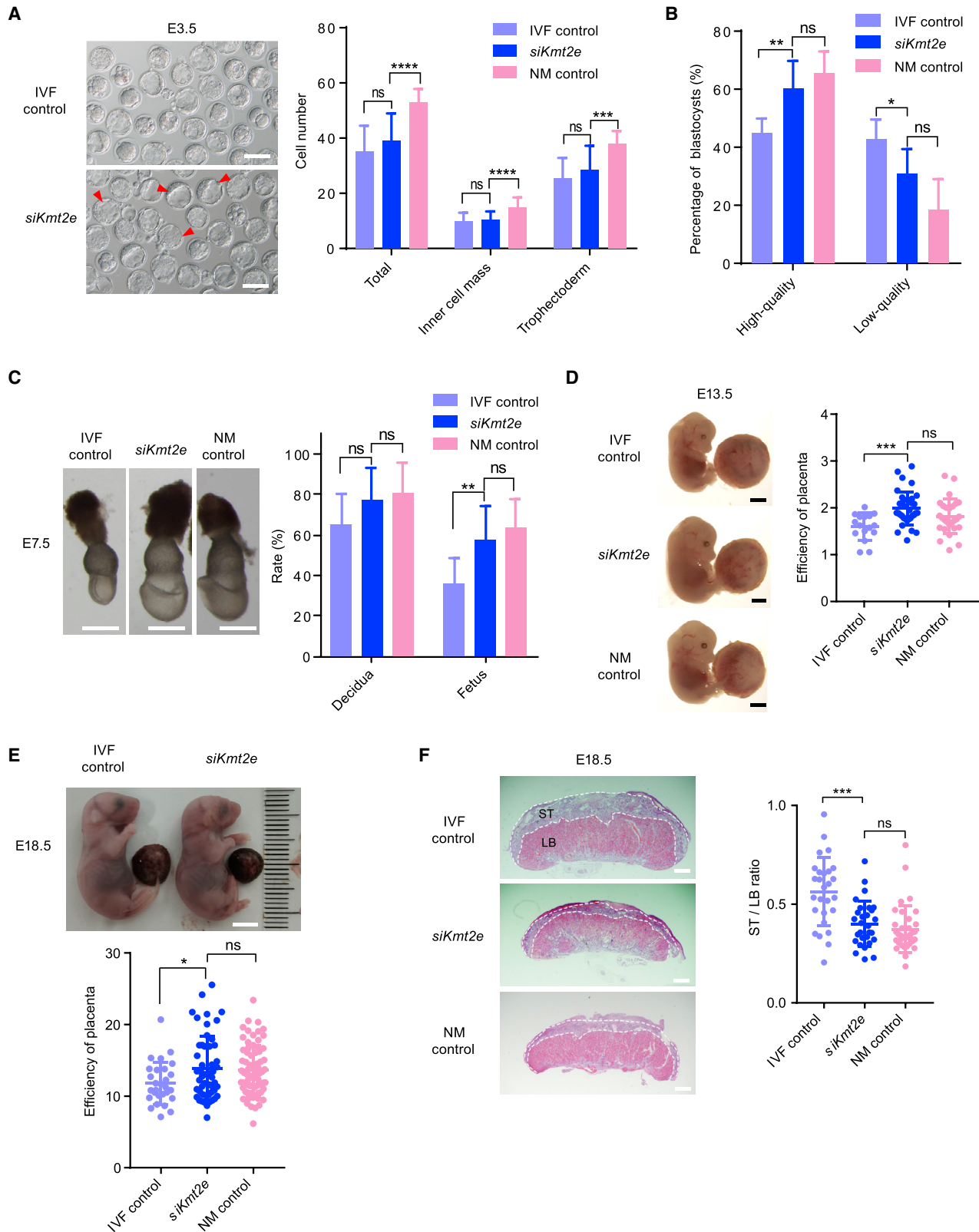
contributes to the fetus and yolk sac, and abnormal development and gene expression lead to defects in post-implantation development. The molecular mechanism of embryonic tissue developmental defects in IVF embryos requires further study.

In summary, our work reveals that the mechanisms of correct histone modification in extraembryonic tissues are critical for embryonic implantation and subsequent placental development. IVF manipulation influences the remodeling of H3K4me3 histone modification in ExE and leads to ectopic lineage-specific gene expression. This study may provide some insights to improve the success rate of IVF and the health of offspring.

Limitations of the study

In our study, to analyze the influence of IVF technology on embryo development, we explored the combined effects of *in vitro* fertilization and *in vitro* culture, but did not explore the effects of *in vitro* fertilization or *in vitro* culture, separately. Meanwhile, we analyzed the transcriptome and histone profile of E3.5 TE without distinguishing polar or parietal trophectoderm despite that ExE is originated from polar TE. Polar TE specialized into ExE and ectoplacental cone (Epc) after implantation, but we did not refer to the defects of Epc in IVF embryos. In our study, we focused on the abnormal development of extraembryonic tissue. Considering the essential role of embryonic tissues for normal embryo development and implantation, improving embryonic tissue development will also help to promote IVF embryo development. The other limitation of our work is that only one differentially expressed H3K4me histone-modifying enzyme was selected and verified in IVF embryos. Thus, other H3K4 methylation regulators that differentially expressed in IVF embryos will be investigated in the future. Finally, whether the pathogenic mechanisms and therapeutic solutions are similar in humans remains to be determined.

STAR★METHODS

Detailed methods are provided in the online version of this paper and include the following:

- ● KEY RESOURCES TABLE
- ● RESOURCE AVAILABILITY
  - ○ Lead contact
  - ○ Materials availability
  - ○ Data and code availability
- ● EXPERIMENTAL MODELS AND SUBJECT DETAILS
  - ○ Animals
- ● METHOD DETAILS
  - ○ Fertilization, culture and embryo collection
  - ○ Histological analyses and immunofluorescence
  - ○ RT-qPCR
  - ○ Single cell collection
  - ○ Smartseq2 RNA-seq and single cell RNA-seq library
  - ○ ULI-NChIP-seq and quantitative ULI-NChIP-seq
  - ○ RNA-seq and ChIP-seq data processing
  - ○ ChromHMM analysis
  - ○ Identification of differentially expressed genes
  - ○ Gene Ontology (GO) analysis
- ● QUANTIFICATION AND STATISTICAL ANALYSIS

AUTHOR CONTRIBUTIONS

W.Q.L., C.Z.J., and S.R.G. conceived and designed the experiments. D.D.B. performed most of the experiments. J.S. performed the computational analysis. C.C., Y.P.J., Y.H.L., K.S.L., Y.L.Z., J.Q.Y., Y.D.L., X.X.H., J.L.R., X.C.K.,

---

Figure 6. Knockdown of *Kmt2e* expression restores the development of IVF extraembryonic tissue

(A) Development and cell numbers of IVF control embryos, *siKmt2e* embryos, and NM control embryos at E3.5. The red arrows (left) denote high-quality blastocysts. The ICM and the TE (right) were identified separately with anti-NONOG and anti-CDX2 antibodies. The cell numbers were counted with ImageJ, and the supporting data are shown in Table S2. Scale bar, 100 μm. The data are presented as the mean ± SD (numbers of total, TE, and ICM cells analyzed: n = 21 for IVF control, n = 34 for *siKmt2e*, n = 16 for NM control). Unpaired Student's t test, ****p < 0.0001, ***p < 0.001.

(B) Percentages of high-quality blastocysts and low-quality blastocysts in the IVF control, *siKmt2e* and NM control groups at E4.5. High-quality blastocysts refer to embryos with dilatation and hatching. Low-quality blastocysts refer to embryos with only dilatation or hatching. The data are presented as the mean ± SD, and the supporting data are shown in Table S1 (for analysis of the percentages of high-quality blastocysts and low-quality blastocysts: n = 6 for IVF control, n = 6 for *siKmt2e*, n = 5 for NM control). Unpaired Student's t test, *p < 0.05, **p < 0.01.

(C) Embryonic development of the IVF control, *siKmt2e*, and NM control groups at E7.5. Scale bar, 500 μm. The data are presented as the mean ± SD, and the supporting data are shown in Table S1 (for analysis of developmental rates of the decidua and fetus: n = 9 for IVF control, n = 8 for *siKmt2e*, n = 9 for NM control). Unpaired Student's t test, **p < 0.01.

(D) Embryonic development of the IVF control, *siKmt2e,* and NM control groups at E13.5. Placental efficiency is the fetal weight/placental weight, and the supporting data are shown in Table S3. Scale bar, 2 mm. The data are presented as the mean ± SD (n = 16 for IVF control, n = 33 for *siKmt2e*, n = 27 for NM control). Unpaired Student's t test, ***p < 0.001.

(E) Embryonic development and placental efficiency of the IVF control, *siKmt2e,* and NM control groups at E18.5. Scale bar, 5 mm. The supporting data are shown in Table S3. The data are presented as the mean ± SD (for analysis of efficiency: n = 28 for IVF control, n = 51 for *siKmt2e*, n = 72 for NM control). Unpaired Student's t test, *p < 0.05.

(F) Placental development of the IVF control, *siKmt2e,* and NM control groups at E18.5. Scale bar, 500 μm. The spongiotrophoblast layer (ST)/labyrinth layer (LB) ratio was used to evaluate the quality of the placenta. The areas of ST and LB were counted with ImageJ, and the supporting data are shown in Table S4. The data are presented as the mean ± SD (n = 27 for IVF control, n = 29 for *siKmt2e*, n = 35 for NM control). Unpaired Student's t test, ***p < 0.001.
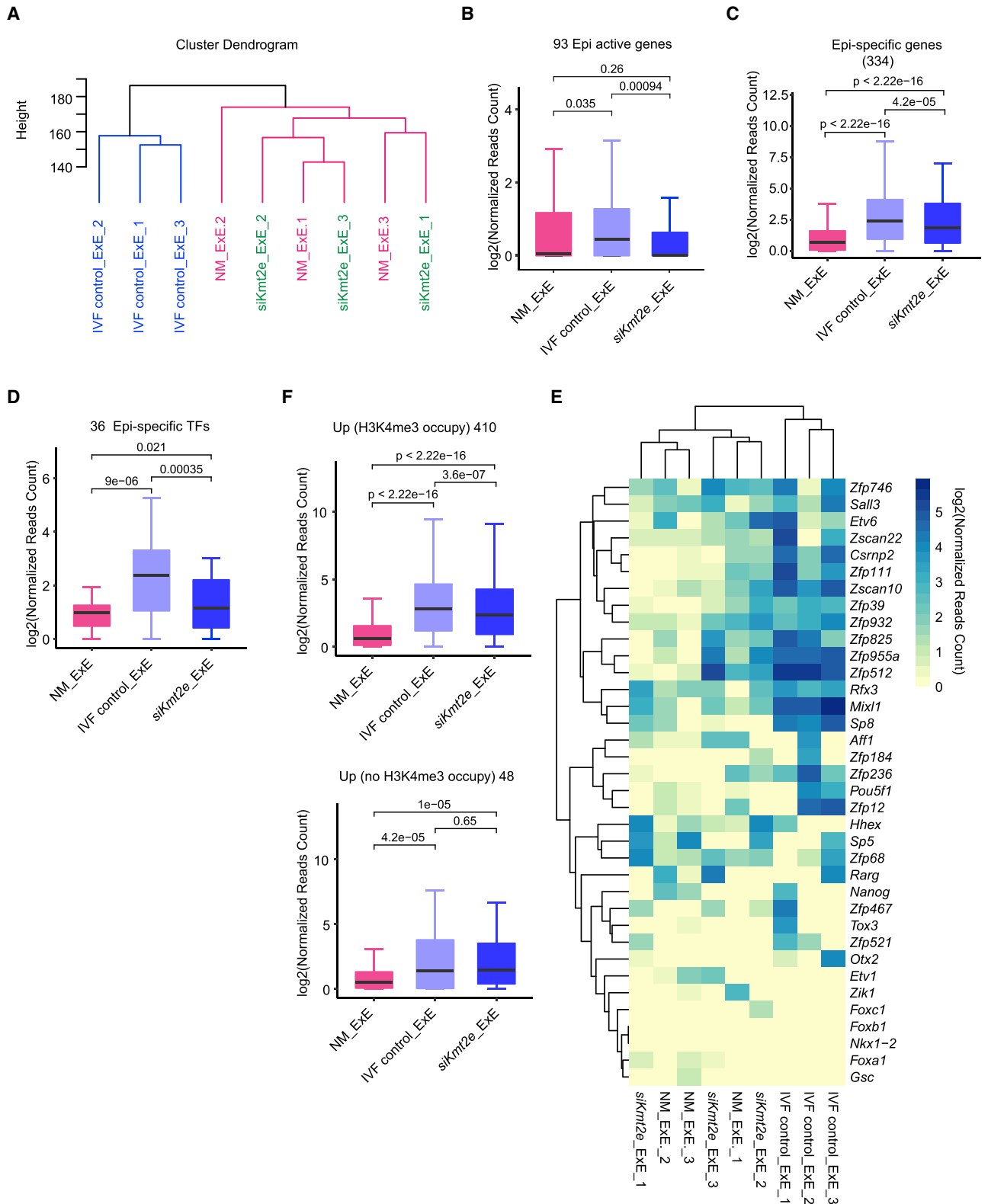
A Cluster Dendrogram

B 93 Epi active genes

C Epi-specific genes (334)

D 36 Epi-specific TFs

F Up (H3K4me3 occupy) 410

Up (no H3K4me3 occupy) 48

E

(legend on next page)

REFERENCES

Ali, M., Rincon-Arano, H., Zhao, W., Rothbart, S.B., Tong, Q., Parkhurst, S.M., Strahl, B.D., Deng, L.W., Groudine, M., and Kutateladze, T.G. (2013). Molecular basis for chromatin binding and regulation of MLL5. Proc. Natl. Acad. Sci. U S A. *110*, 11296–11301. https://doi.org/10.1073/pnas.1310156110.

Apicella, C., Ruano, C.S.M., Mehats, C., Miralles, F., and Vaiman, D. (2019). The role of epigenetics in placental development and the etiology of preeclampsia. Int. J. Mol. Sci. *20*, 2837. https://doi.org/10.3390/ijms20112837.

Arima, T., Hata, K., Tanaka, S., Kusumi, M., Li, E., Kato, K., Shiota, K., Sasaki, H., and Wake, N. (2006). Loss of the maternal imprint in Dnmt3L(mat-/-) mice leads to a differentiation defect in the extraembryonic tissue. Dev. Biol. *297*, 361–373. https://doi.org/10.1016/j.ydbio.2006.05.003.

Bai, X., Zheng, C.Y., and Ma, M. (2019). Pharmacological modulation of autophagy as a novel potential target in the successful implementation of in vitro fertilization. Life Sci. *229*, 93–97. https://doi.org/10.1016/j.lfs.2019.05.032.

Benayoun, B.A., Pollina, E.A., Ucar, D., Mahmoudi, S., Karra, K., Wong, E.D., Devarajan, K., Daugherty, A.C., Kundaje, A.B., Mancini, E., et al. (2014). H3K4me3 breadth is linked to cell identity and transcriptional consistency. Cell *158*, 673–688. https://doi.org/10.1016/j.cell.2014.06.027.

Bloise, E., Lin, W.K., Liu, X.W., Simbulan, R., Kolahi, K.S., Petraglia, F., Maltepe, E., Donjacour, A., and Rinaudo, P. (2012). Impaired placental nutrient transport in mice generated by in vitro fertilization. Endocrinology *153*, 3457–3467. https://doi.org/10.1210/en.2011-1921.

Brind'Amour, J., Liu, S., Hudson, M., Chen, C., Karimi, M.M., and Lorincz, M.C. (2015). An ultra-low-input native ChIP-seq protocol for genome-wide profiling of rare cell populations. Nat. Commun. *6*, 6033. https://doi.org/10.1038/ncomms7033.

Brown, L.Y., Bonney, E.A., Raj, R.S., Nielsen, B., and Brown, S. (2013). Generalized disturbance of DNA methylation in the uterine decidua in the CBA/J x DBA/2 mouse model of pregnancy failure. Biol. Reprod. *89*, 120.

Bu, Z.Q., Hu, L.L., Su, Y.C., Guo, Y.H., Zhai, J., and Sun, Y.P. (2020). Factors related to early spontaneous miscarriage during IVF/ICSI treatment: an analysis of 21,485 clinical pregnancies. Reprod. Biomed. Online *40*, 201–206. https://doi.org/10.1016/j.rbmo.2019.11.001.

Chen, K.F., Chen, Z., Wu, D.Y., Zhang, L.L., Lin, X.Q., Su, J.Z., Rodriguez, B., Xi, Y.X., Xia, Z., Chen, X., et al. (2015). Broad H3K4me3 is associated with increased transcription elongation and enhancer activity at tumor-suppressor genes. Nat. Genet. *47*, 1149–1157. https://doi.org/10.1038/ng.3385.

Cleaton, M.A.M., Edwards, C.A., and Ferguson-Smith, A.C. (2014). Phenotypic outcomes of imprinted gene models in mice: elucidation of pre- and postnatal functions of imprinted genes. Annu. Rev. Genom Hum. G *15*, 93–126. https://doi.org/10.1146/annurev-genom-091212-153441.

Dahl, J.A., Jung, I., Aanes, H., Greggains, G.D., Manaf, A., Lerdrup, M., Li, G.Q., Kuan, S., Li, B., Lee, A.Y., et al. (2016). Broad histone H3K4me3 domains in mouse oocytes modulate maternal-to-zygotic transition. Nature *537*, 548–552. https://doi.org/10.1038/nature19360.

de Waal, E., Mak, W., Calhoun, S., Stein, P., Ord, T., Krapp, C., Coutifaris, C., Schultz, R.M., and Bartolomei, M.S. (2014). *In vitro* culture increases the frequency of stochastic epigenetic errors at imprinted genes in placental tissues from mouse concepti produced through assisted reproductive technologies. Biol. Reprod. *90*, 22.

de Waal, E., Vrooman, L.A., Fischer, E., Ord, T., Mainigi, M.A., Coutifaris, C., Schultz, R.M., and Bartolomei, M.S. (2015). The cumulative effect of assisted reproduction procedures on placental development and epigenetic perturbations in a mouse model. Hum. Mol. Genet. *24*, 6975–6985. https://doi.org/10.1093/hmg/ddv400.

Duranthon, V., and Chavatte-Palmer, P. (2018). Long term effects of ART: what do animals tell us? Mol. Reprod. Dev. *85*, 348–368. https://doi.org/10.1002/mrd.22970.

Ernst, J., and Kellis, M. (2012). ChromHMM: automating chromatin-state discovery and characterization. Nat. Methods *9*, 215–216. https://doi.org/10.1038/nmeth.1906.

Ernst, J., and Kellis, M. (2017). Chromatin-state discovery and genome annotation with ChromHMM. Nat. Protoc. *12*, 2478–2492. https://doi.org/10.1038/nprot.2017.124.

Eroglu, A., and Layman, L.C. (2012). Role of ART in imprinting disorders. Semin. Reprod. Med. *30*, 092–104. https://doi.org/10.1055/s-0032-1307417.

Fauser, B.C.J.M., Devroey, P., Diedrich, K., Balaban, B., Bonduelle, M., Delemarre-van de Waal, H.A., Estella, C., Ezcurra, D., Geraedts, J.P.M., Howles, C.M., et al. (2014). Health outcomes of children born after IVF/ICSI: a review of current expert opinion and literature. Reprod. Biomed. Online *28*, 162–182. https://doi.org/10.1016/j.rbmo.2013.10.013.

Fowden, A.L., Coan, P.M., Angiolini, E., Burton, G.J., and Constancia, M. (2011). Imprinted genes and the epigenetic regulation of placental phenotype. Prog. Biophys. Mol. Bio *106*, 281–288. https://doi.org/10.1016/j.pbiomolbio.2010.11.005.

Guo, X.Y., Liu, X.M., Jin, L., Wang, T.T., Ullah, K., Sheng, J.Z., and Huang, H.F. (2017). Cardiovascular and metabolic profiles of offspring conceived by assisted reproductive technologies: a systematic review and meta-analysis. Fertil. Steril *107*, 622–631.e5. https://doi.org/10.1016/j.fertnstert.2016.12.007.

Hanna, C.W., Perez-Palacios, R., Gahurova, L., Schubert, M., Krueger, F., Biggins, L., Andrews, S., Colome-Tatche, M., Bourc'his, D., Dean, W., and Kelsey, G. (2019). Endogenous retroviral insertions drive non-canonical imprinting in extra-embryonic tissues. Genome Biol. *20*, 225. https://doi.org/10.1186/s13059-019-1833-x.

Hansen, P.J. (2020). Implications of assisted reproductive technologies for pregnancy outcomes in mammals. Annu. Rev. Anim. Biosci. *8*, 395–413. https://doi.org/10.1146/annurev-animal-021419-084010.

Hayward, C.E., Lean, S., Sibley, C.P., Jones, R.L., Wareing, M., Greenwood, S.L., and Dilworth, M.R. (2016). Placental adaptation: what can we learn from birthweight:placental weight ratio? Front. Physiol. *7*, 28. https://doi.org/10.3389/fphys.2016.00028.

Hu, L.M., Du, J.B., Lv, H., Zhao, J., Chen, M.X., Wang, Y.F., Wu, F., Liu, F., Chen, X.J., Zhang, J.Q., et al. (2018). Influencing factors of pregnancy loss and survival probability of clinical pregnancies conceived through assisted

Figure 7. *Kmt2e* interference ameliorates the changes in lineage-specific gene expression in IVF ExE tissue

(A) Gene expression cluster in ExE of the NM, IVF control, and *siKmt2e* groups.
(B) Expression of 93 Epi active genes in ExE of the NM, IVF control, and *siKmt2e* groups.
(C) Expression of 334 Epi-specific genes in ExE of the NM, IVF control, and *siKmt2e* groups.
(D) Expression of 36 Epi-specific TFs in ExE of the NM, IVF control, and *siKmt2e* groups.
(E) Heatmap showing the expression and clustering of 36 Epi-specific TFs in the ExE of the NM, IVF control, and *siKmt2e* groups.
(F) Expression of 410 upregulated genes (with H3K4me3 occupancy) and 48 upregulated genes (without H3K4me3 occupancy) in ExE of the NM, IVF control, and *siKmt2e* groups.

reproductive technology. Reprod. Biol. Endocrin 16, 74. https://doi.org/10.1186/s12958-018-0390-6.

Huang, J.J., Zhang, H.Y., Wang, X.L., Dobbs, K.B., Yao, J., Qin, G.S., Whitworth, K., Walters, E.M., Prather, R.S., and Zhao, J.G. (2015). Impairment of preimplantation porcine embryo development by histone demethylase KDM5B knockdown through disturbance of bivalent H3K4me3-H3K27me3 modifications. Biol. Reprod. 92, 72. https://doi.org/10.1095/biolreprod.114.122762.

Inoue, A., Jiang, L., Lu, F.L., Suzuki, T., and Zhang, Y. (2017). Maternal H3K27me3 controls DNA methylation-independent imprinting. Nature 547, 419–424. https://doi.org/10.1038/nature23262.

Iwagawa, T., and Watanabe, S. (2019). Molecular mechanisms of H3K27me3 and H3K4me3 in retinal development. Neurosci. Res. 138, 43–48. https://doi.org/10.1016/j.neures.2018.09.010.

Jauniaux, E., Moffett, A., and Burton, G.J. (2020). Placental implantation disorders. Obstet. Gyn Clin. N. Am. 47, 117–132. https://doi.org/10.1016/j.ogc.2019.10.002.

Kim, D., Langmead, B., and Salzberg, S.L. (2015). HISAT: a fast spliced aligner with low memory requirements. Nat. Methods 12, 357–360. https://doi.org/10.1038/nmeth.3317.

Lee, G.K., Shin, H., and Lim, H.J. (2016). Rapamycin influences the efficiency of in vitro fertilization and development in the mouse: a role for autophagic activation. Asian Austral J. Anim. 29, 1102–1110. https://doi.org/10.5713/ajas.15.0762.

Li, H., and Durbin, R. (2009). Fast and accurate short read alignment with Burrows-Wheeler transform. Bioinformatics 25, 1754–1760. https://doi.org/10.1093/bioinformatics/btp324.

Liao, Y., Smyth, G.K., and Shi, W. (2014). featureCounts: an efficient general purpose program for assigning sequence reads to genomic features. Bioinformatics 30, 923–930. https://doi.org/10.1093/bioinformatics/btt656.

Liu, J., An, L.Y., Wang, J.Q., Liu, Z.H., Dai, Y.J., Liu, Y.H., Yang, L., and Du, F.L. (2019). Dynamic patterns of H3K4me3, H3K27me3, and Nanog during rabbit embryo development. Am. J. Transl Res. 11, 430–441.

Liu, X.Y., Wang, C.F., Liu, W.Q., Li, J.Y., Li, C., Kou, X.C., Chen, J.Y., Zhao, Y.H., Gao, H.B., Wang, H., et al. (2016). Distinct features of H3K4me3 and H3K27me3 chromatin domains in pre-implantation embryos. Nature 537, 558–562. https://doi.org/10.1038/nature19362.

Love, M.I., Huber, W., and Anders, S. (2014). Moderated estimation of fold change and dispersion for RNA-seq data with DESeq2. Genome Biol. 15, 550. https://doi.org/10.1186/s13059-014-0550-8.

Ma, Z.J., Wang, H., Cai, Y.P., Wang, H., Niu, K.Y., Wu, X.F., Ma, H.H., Yang, Y., Tong, W.H., Liu, F., et al. (2018). Epigenetic drift of H3K27me3 in aging links glycolysis to healthy longevity in Drosophila. Elife 7, e35368. https://doi.org/10.7554/elife.35368.

Madan, V., Madan, B., Brykczynska, U., Zilbermann, F., Hogeveen, K., Dohner, K., Dohner, H., Weber, O., Blum, C., Rodewald, H.R., et al. (2009). Impaired function of primitive hematopoietic cells in mice lacking the Mixed-Lineage-Leukemia homolog Mll5. Blood 113, 1444–1454. https://doi.org/10.1182/blood-2008-02-142638.

Mascarenhas, M.N., Flaxman, S.R., Boerma, T., Vanderpoel, S., and Stevens, G.A. (2012). National, regional, and global trends in infertility prevalence since 1990: a systematic analysis of 277 health surveys. PLoS Med. 9, e1001356. https://doi.org/10.1371/journal.pmed.1001356.

Meng, M., Liu, H.F., Chen, S.D., Zhao, H.J., Gao, X., Zhang, J.N., and Chen, D.Z. (2019). Methylation of H3K27 and H3K4 in key gene promoter regions of thymus in RA mice is involved in the abnormal development and differentiation of iNKT cells. Immunogenetics 71, 489–499. https://doi.org/10.1007/s00251-019-01124-x.

Movahed, E., Shabani, R., Hosseini, S., Shahidi, S., and Salehi, M. (2020). Interfering effects of in vitro fertilization and vitrification on expression of Gtl2 and Dlk1 in mouse blastocysts. Int. J. Fertil. Steril 14, 110–115. https://doi.org/10.22074/ijfs.2020.5984.

Orlando, D.A., Chen, M.W., Brown, V.E., Solanki, S., Choi, Y.J., Olson, E.R., Fritz, C.C., Bradner, J.E., and Guenther, M.G. (2014). Quantitative ChIP-seq normalization reveals global modulation of the epigenome. Cell Rep 9, 1163–1170. https://doi.org/10.1016/j.celrep.2014.10.018.

Park, S., Kim, G.W., Kwon, S.H., and Lee, J.S. (2020). Broad domains of histone H3 lysine 4 trimethylation in transcriptional regulation and disease. Febs J. 287, 2891–2902. https://doi.org/10.1111/febs.15219.

Picelli, S., Faridani, O.R., Bjorklund, A.K., Winberg, G., Sagasser, S., and Sandberg, R. (2014). Full-length RNA-seq from single cells using Smartseq2. Nat. Protoc. 9, 171–181. https://doi.org/10.1038/nprot.2014.006.

Quinlan, A.R., and Hall, I.M. (2010). BEDTools: a flexible suite of utilities for comparing genomic features. Bioinformatics 26, 841–842. https://doi.org/10.1093/bioinformatics/btq033.

Ramirez, F., Ryan, D.P., Gruning, B., Bhardwaj, V., Kilpert, F., Richter, A.S., Heyne, S., Dundar, F., and Manke, T. (2016). deepTools2: a next generation web server for deep-sequencing data analysis. Nucleic Acids Res. 44, W160–W165. https://doi.org/10.1093/nar/gkw257.

Robinson, M.D., McCarthy, D.J., and Smyth, G.K. (2010). edgeR: a Bioconductor package for differential expression analysis of digital gene expression data. Bioinformatics 26, 139–140. https://doi.org/10.1093/bioinformatics/btp616.

Sebastian, S., Sreenivas, P., Sambasivan, R., Cheedipudi, S., Kandalla, P., Pavlath, G.K., and Dhawan, J. (2009). MLL5, a trithorax homolog, indirectly regulates H3K4 methylation, represses cyclin A2 expression, and promotes myogenic differentiation. Proc. Natl. Acad. Sci. U S A. 106, 4719–4724. https://doi.org/10.1073/pnas.0807136106.

Shen, X.H., Zhang, N., Wang, Z.D., Bai, G.Y., Zheng, Z., Gu, Y.L., Wu, Y.S., Liu, H., Zhou, D.J., and Lei, L. (2015). Induction of autophagy improves embryo viability in cloned mouse embryos. Sci. Rep. 5, 17829. https://doi.org/10.1038/srep17829.

Shinar, S. (2018). Reply to letter to the editor. Arch. Gynecol. Obstet. 298, 1229. https://doi.org/10.1007/s00404-018-4904-4.

Smith, F.M., Garfield, A.S., and Ward, A. (2006). Regulation of growth and metabolism by imprinted genes. Cytogenet. Genome Res. 113, 279–291. https://doi.org/10.1159/000090843.

Tan, K., Zhang, Z.N., Miao, K., Yu, Y., Sui, L.L., Tian, J.H., and An, L. (2016). Dynamic integrated analysis of DNA methylation and gene expression profiles in vivo and in vitro fertilized mouse post-implantation extraembryonic and placental tissues. Mol. Hum. Reprod. 22, 485–498. https://doi.org/10.1093/molehr/gaw028.

Tang, F.C., Barbacioru, C., Nordman, E., Li, B., Xu, N.L., Bashkirov, V.I., Lao, K.Q., and Surani, M.A. (2010). RNA-Seq analysis to capture the transcriptome landscape of a single cell. Nat. Protoc. 5, 516–535. https://doi.org/10.1038/nprot.2009.236.

Tang, F.C., Barbacioru, C., Wang, Y.Z., Nordman, E., Lee, C., Xu, N.L., Wang, X.H., Bodeau, J., Tuch, B.B., Siddiqui, A., et al. (2009). mRNA-Seq whole-transcriptome analysis of a single cell. Nat. Methods 6, 377–382. https://doi.org/10.1038/nmeth.1315.

Tunster, S.J., McNamara, G.I., Creeth, H.D.J., and John, R.M. (2016). Increased dosage of the imprinted Ascl2 gene restrains two key endocrine lineages of the mouse Placenta. Dev. Biol. 418, 55–65. https://doi.org/10.1016/j.ydbio.2016.08.014.

Vander Borght, M., and Wyns, C. (2018). Fertility and infertility: definition and epidemiology. Clin. Biochem. 62, 2–10. https://doi.org/10.1016/j.clinbiochem.2018.03.012.

Vastenhouw, N.L., and Schier, A.F. (2012). Bivalent histone modifications in early embryogenesis. Curr. Opin. Cell Biol 24, 374–386. https://doi.org/10.1016/j.ceb.2012.03.009.

Ventura-Junca, P., Irarrazaval, I., Rolle, A.J., Gutierrez, J.I., Moreno, R.D., and Santos, M.J. (2015). In vitro fertilization (IVF) in mammals: epigenetic and developmental alterations. Scientific and bioethical implications for IVF in humans. Biol. Res. 48, 68. https://doi.org/10.1186/s40659-015-0059-y.

von Wolff, M., and Haaf, T. (2020). *In vitro* fertilization technology and child health. Dtsch Arztebl Int. *117*, 23–30. https://doi.org/10.3238/arztebl.2020.0023.

Xiang, Y.L., Zhang, Y., Xu, Q.H., Zhou, C., Liu, B.F., Du, Z.H., Zhang, K., Zhang, B.J., Wang, X.X., Gayen, S., et al. (2020). Epigenomic analysis of gastrulation identifies a unique chromatin state for primed pluripotency. Nat. Genet. *52*, 95–105. https://doi.org/10.1038/s41588-019-0545-1.

Yang, X.F., Hu, B.Q., Hou, Y., Qiao, Y.B., Wang, R., Chen, Y.Y., Qian, Y., Feng, S., Chen, J., Liu, C., et al. (2018). Silencing of developmental genes by H3K27me3 and DNA methylation reflects the discrepant plasticity of embryonic and extraembryonic lineages. Cell Res *28*, 593–596. https://doi.org/10.1038/s41422-018-0010-1.

Yin, L.J., Zhang, Y., Lv, P.P., He, W.H., Wu, Y.T., Liu, A.X., Ding, G.L., Dong, M.Y., Qu, F., Xu, C.M., et al. (2012). Insufficient maintenance DNA methylation is associated with abnormal embryonic development. Bmc Med. *10*, 26. https://doi.org/10.1186/1741-7015-10-26.

Zeadna, A., Son, W.Y., Moon, J.H., and Dahan, M.H. (2015). A comparison of biochemical pregnancy rates between women who underwent IVF and fertile controls who conceived spontaneously. Hum. Reprod. *30*, 783–788. https://doi.org/10.1093/humrep/dev024.

Zhang, B.J., Zheng, H., Huang, B., Li, W.Z., Xiang, Y.L., Peng, X., Ming, J., Wu, X.T., Zhang, Y., Xu, Q.H., et al. (2016). Allelic reprogramming of the histone modification H3K4me3 in early mammalian development. Nature *537*, 553–557. https://doi.org/10.1038/nature19361.

Zhang, X.M., Novera, W., Zhang, Y., and Deng, L.W. (2017). MLL5 (KMT2E): structure, function, and clinical relevance. Cell Mol Life Sci *74*, 2333–2344. https://doi.org/10.1007/s00018-017-2470-8.

Zhang, Y., Liu, T., Meyer, C.A., Eeckhoute, J., Johnson, D.S., Bernstein, B.E., Nusbaum, C., Myers, R.M., Brown, M., Li, W., and Liu, X.S. (2008). Model-based analysis of ChIP-seq (MACS). Genome Biol. *9*, R137. https://doi.org/10.1186/gb-2008-9-9-r137.

Zhou, Y., Zhou, B., Pache, L., Chang, M., Khodabakhshi, A.H., Tanaseichuk, O., Benner, C., and Chanda, S.K. (2019). Metascape provides a biologist-oriented resource for the analysis of systems-level datasets. Nat. Commun. *10*, 1523. https://doi.org/10.1038/s41467-019-09234-6.

STAR★METHODS

KEY RESOURCES TABLE

REAGENT or RESOURCE	SOURCE	IDENTIFIER
Antibodies		
Mouse anti-CDX2	Bio-Genex	Cat# MU392A-UC; RRID: AB_2335627
Rabbit anti-NANOG	Reprocell	Cat# RCAB002P-F; RRID:AB_1560380
Rabbit anti-H3K4me3	Cell signaling Technology	Cat# 9727S; RRID:AB_561095
Rabbit anti-H3K27me3	Diagnode	Cat# C15410195; RRID: AB_2753161
Donkey anti-Rabbit IgG (H + L) Highly Cross-Adsorbed Secondary Antibody, Alexa Fluor 488	Invitrogen	Cat# A21206; RRID:AB_2535792
Donkey anti-Mouse IgG (H + L) Highly Cross-Adsorbed Secondary Antibody, Alexa Fluor 594	Invitrogen	Cat# A21203; RRID:AB_141633
Chemicals, peptides, and recombinant proteins		
Pronase E (Protease from Streptomyces griseus)	Sigma	Cat# P8811
Trypsin-EDTA	Gibco	Cat# 25300062
Pregnant mare serum gonadotropin (PMSG)	San-Sheng	N/A
Human chorionic gonadotropin (hCG)	San-Sheng	N/A
G-IVF PLUS medium	Vitrolife	Cat# 10,136
G-1 PLUS medium	Vitrolife	Cat# 10128
BSA (bovine serum albumin)	MP Biomedicals	Cat# 180549
0.5% Triton X-100	Sigma	Cat# 93443
DAPI (4′,6-diamidino-2-phenylindole)	Invitrogen	Cat# D3571
4% paraformaldehyde (PFA)	Servicebio	Cat# G1101
Critical commercial assays		
5× All-In-One RT MasterMix	ABM	Cat# G490
Chamq Universal SYBR qPCR Master Mix	Vazyme	Cat# Q711-02
Kapa Hyper Prep Kit	KAPA	Cat# kk8504
Deposited data		
ULI-NChIP-Seq data and quantitative ULI-NChIP-Seq of H3K4me3 and H3K27me3 of NM, IVF, NM control and *siKdm5b* groups	This paper	GEO: GSE168274
Single cell RNA-seq data of NM and IVF groups	This paper	GEO: GSE168274
Smartseq2 RNA-seq data of NM control, IVF control, *siKdm5b* and *siKmt2e* groups	This paper	GEO: GSE168274
Experimental models: organisms/strains		
Mouse: C57BL/6N	Charles River	N/A
Mouse: ICR	Charles River	N/A
Mouse: DBA2	Charles River	N/A
Oligonucleotides		
qPCR primers and siRNA sequence (see Table S7)	This paper	N/A
Software and algorithms		
ImageJ/Fiji	N/A	imagej.nih.gov/ij/download.html
Bwa (0.7.12-r1039)	(Li and Durbin, 2009)	http://bio-bwa.sourceforge.net/
HISAT2 (version 2.1.0)	(Kim et al., 2015)	http://daehwankimlab.github.io/hisat2/manual/
BEDtools (v2.25.0)	(Quinlan and Hall, 2010)	https://bedtools.readthedocs.io/en/latest/
Samtools (1.9)	(Li and Durbin, 2009)	http://www.htslib.org/
Picard (1.138)	N/A	https://broadinstitute.github.io/picard/

(Continued on next page)

Continued

REAGENT or RESOURCE	SOURCE	IDENTIFIER
deeptools (2.5.7)	(Ramirez et al., 2016)	https://deeptools.readthedocs.io/en/develop/
Metascape	(Zhou et al., 2019)	http://metascape.org/gp/index.html
DESeq2 (1.18.1)	(Love et al., 2014)	https://bioconductor.org/packages/release/bioc/html/DESeq2.html
Cutadapt (version 2.5)	N/A	https://cutadapt.readthedocs.io/en/stable/
featureCounts (Version 1.6.1)	(Liao et al., 2014)	http://subread.sourceforge.net/
ChromHMM (Version 1.15)	(Ernst and Kellis, 2017)	http://compbio.mit.edu/ChromHMM/
MACS2 (2.1.2)	(Zhang et al., 2008)	https://pypi.org/project/MACS2/
edgeR (3.20.9)	(Robinson et al., 2010)	https://bioconductor.org/packages/release/bioc/html/edgeR.html
Other		
7500 Fast Real-Time PCR System	Applied BioSystems	ABI7500
Covaris S220	Covaris	S220
U-HGLGPS	Olympus	N/A
Microscope	Olympus	IX73

RESOURCE AVAILABILITY

Lead contact
Further information and requests for resources and reagents should be directed to and will be fulfilled by the Lead Contact, Shaorong Gao (gaoshaorong@tongji.edu.cn).

Materials availability
This study did not generate new unique reagents.

Data and code availability
- ULI-NChIP-Seq data, quantitative ULI-NChIP-Seq data, single cell RNA-seq data and Smartseq2 RNA-seq data generated in this study have been deposited at the Gene Expression Omnibus and are publicly available at the date of publication. Accession number is listed in the Key resources table.
- This paper does not report original code.
- Any additional information required to reanalyze the data reported in this paper is available from the Lead contact upon request.

EXPERIMENTAL MODELS AND SUBJECT DETAILS

Animals
The mice were housed in a specific pathogen-free (SPF) animal facility at Tongji University, Shanghai, China. Adult female (6–8 weeks old) and adult male (8–10 weeks old) B6D2F1 (C57BL/6 female × DBA2 male) mice were used as donors for oocytes and sperm. ICR adult females (8–10 weeks old) were used as pseudopregnant receptors. All experimental steps and animal breeding procedures were carried out in accordance with the Tongji University experimental animal use guide.

METHOD DETAILS

Fertilization, culture and embryo collection
Superovulation was implemented for B6D2F1 female mice. The mice were intraperitoneally injected with 5 IU of pregnant mare serum gonadotropin (PMSG) (San-Sheng, China) and with 7 IU of human chorionic gonadotropin (hCG) (San-Sheng) 48 h later. Superovulated females were mated with B6D2F1 males or subjected to IVF procedures. Briefly, cumulus-oocyte complexes were collected from the oviducts 13–14 h after hCG injection. Sperm obtained from B6D2F1 males were capacitated for 20–30 min in G-IVF PLUS medium (Vitrolife, Sweden) in a 37°C cell incubator containing 5% CO_2. *In vitro* fertilization (IVF) was performed with the cumulus-oocyte complexes and capacitated sperm in G-IVF PLUS medium (Vitrolife) under mineral oil for 5 h in a 37°C cell incubator containing 5% CO2. Then, fertilized eggs were transferred into G-1 PLUS medium (Vitrolife, Sweden) under mineral oil until the blastocyst stage. Blastocysts collected from the G-1 PLUS medium (Vitrolife) and mated B6D2F1 female mice were transferred into the uteri of pseudopregnant ICR females. Embryos at the 2-cell, morula and blastocyst stages of the natural mated group were collected

from the oviducts or uteri of mated B6D2F1 female mice. Preimplantation embryos from IVF were collected from the G-1 PLUS medium (Vitrolife). Embryos were collected from the surrogate mothers at E7.5, E13.5 and E18.5.

Histological analyses and immunofluorescence

Placentas collected at E18.5 were fixed overnight with 4% paraformaldehyde (Servicebio, China) at 4°C. After fixation, the placentas were embedded in paraffin and cut along the largest longitudinal cross-sections. The sections were stained with hematoxylin and eosin (H&E) and photographed with a microscope. The areas of the decidua, spongiotrophoblast layer and labyrinth layer were counted using ImageJ software.

Blastocysts were fixed with 4% paraformaldehyde (Servicebio) overnight at 4°C. After fixation, the samples were permeabilized with 0.5% Triton X-100 (Sigma, Germany) for 5 min at room temperature. Then, the samples were blocked with 3% bovine serum albumin (BSA)-PBS (MP Biomedicals, USA) for 1–2 h at room temperature. The samples were incubated with primary antibodies against CDX2 (1:800, Bio-Genex, MU392A-UC, USA) and NANOG (1:500, Reprocell, RCAB002P-F, Japan) overnight at 4°C. The samples were then washed 3 times with 1% BSA-PBS (MP Biomedicals) and incubated with anti-mouse and anti-rabbit secondary antibodies at room temperature for 1 h 4′,6-diamidino-2-phenylindole (DAPI) (Invitrogen, D3571) was used to stain nuclei for 15–20 min at room temperature. All prepared samples were observed and photographed with a fluorescence microscope.

RT-qPCR

A total of 100–200 blastocysts were used to collect RNA by the phenol chloroform extraction method. cDNA was synthesized using 5x All-In-One RT Master Mix (Abm, G490, Canada). Quantitative PCR (QPCR) was performed using Chamq Universal SYBR qPCR Master Mix (Vazyme, Q711-02, China). The signals were detected using a real-time PCR system (ABI7500, Applied BioSystems, USA). *Hprt* was used as an endogenous control. The results were analyzed with GraphPad Prism 7 software.

Single cell collection

Single cells of preimplantation embryos were collected without polar bodies by removing the zone pellucida with 20 mg/ml PE (Pronase E, Sigma), incubating in CZB without Ca^{2+} and gently pipetting with a fire-polished glass tube. Single cells of E7.5 embryos (ExE, Epi) were collected by separation from the decidua and digestion with 0.05% trypsin-EDTA (Gibco, 25300062). All the cells were washed at least three times with 0.5% BSA-PBS (MP Biomedicals) solution before use.

Smartseq2 RNA-seq and single cell RNA-seq library

According to previous methods, approximately 10–20 cells were used to construct each library (Picelli et al., 2014; Tang et al., 2009, 2010). The prepared cells were transferred to lysis buffer by mouth pipetting. Reverse transcription was performed directly using oligo (dT) primers in lysates containing complete cytoplasm. Second-strand cDNA was synthesized depending on the poly(A) tail attached to the 3′ end of the first-strand cDNA or via template switching with a TSO. Fragment cDNA was prepared for sequence library construction using a Covaris sonicator (Covaris S220, Woburn, MA, USA). A Kapa Hyper Prep Kit (KAPA, KK8504, Switzerland) was used to complete the sequence libraries. The libraries were sequenced on Illumina HiSeq 2500, Illumina HiSeq X10 and Illumina NovaSeq instruments with paired-end reads of 125 bp or 150 bp. Quality control and sequencing were performed by Berry, Novogene and ANOROAD Genomics Corporation.

ULI-NChIP-seq and quantitative ULI-NChIP-seq

According to previous studies, approximately 500–1000 cells were used per library (Brind'Amour et al., 2015; Liu et al., 2016). Approximately 1 μg of histone H3K4me3 antibody (Cell Signaling Technology, 9727S, USA) or histone H3K27me3 antibody (Diagnode, C15410195, Belgium) was used for the immunoprecipitation reaction. The ULI-NChIP-seq libraries were generated with a Kapa Hyper Prep Kit (KAPA, KK8504, Switzerland).

Quantitative ULI-NChIP-Seq was performed by adding 5% human cells 293T during the sample collection stage and the other steps was same as ULI-NChIP-seq (Ma et al., 2018; Orlando et al., 2014).

The libraries were sequenced on an Illumina HiSeq 2500 and Illumina NovaSeq 6000 with 125 bp single- or paired-end sequences. Quality control and sequencing were performed by Berry, Novogene and ANOROAD Genomics Corporation.

RNA-seq and ChIP-seq data processing

The mRNA-seq reads were first trimmed with an Illumina universal adapter using Cutadapt version 2.5 with the default parameters and then aligned to the mm9 transcript reference genome using HISAT2 version 2.1.0 with the parameters (Kim et al., 2015). Only uniquely mapped reads were used for downstream analyses. The reads mapped to each gene were counted using featureCounts version 1.6.1 with the default parameters and iGenome mm9 gene annotation (Liao et al., 2014). The abundance of each gene was quantified using edgeR version 3.4.3, and the log2(normalized read count +1) was used as the normalized gene expression (Robinson et al., 2010). DEGs were defined with stringent cutoffs of a p.adj <0.01 and a log2(fold change) > 2 using the R package DESeq2 (Love et al., 2014). The ChIP-seq reads were aligned to mm9 using the bwa version 0.7.12 mem command (Li and Durbin, 2009). PCR duplicates were removed using Picard (https://broadinstitute.github.io/picard/), and only high-quality mapped reads (MAPQ>20) were retained for downstream analyses. Signal tracks were generated using MACS2 version 2.1.2 and normalized using the logFE method (Zhang et al., 2008).

ChromHMM analysis

Chromatin states were identified and characterized using ChromHMM version 1.15 (Ernst and Kellis, 2017). The alignment files of H3K4me3 and H3K27me3 were binned into 500 bp bins using the BinarizeBam command, with the input alignment file as the control, and the model was trained with 4 emission states using a 500 bp resolution and the default parameters using the LearnModel command. The whole genome was classified into two states: the H3K4me3 state and the H3K27me3 state. Regions with the same state were merged with BEDtools version 2.25.0, and the state were redefined on the basis of four possible states: the H3K4me3-only state (without H3K27me3), the H3K27me3-only state (without H3K4me3), the bivalent state (in which the H3K4me3 region intersected the H3K27me3 region), and the unmarked state (Quinlan and Hall, 2010).

The promoter was defined as the area within ±1 kb of the TSS, and its state was determined on the basis of the closest region (unless unmarked) upstream of the TSS that intersected with the promoter; otherwise, the state was determined to be unmarked. The dHM state regions were defined using the top 5% differentially marked regions.

Identification of differentially expressed genes

The differentially expressed genes in Figure 2C for the IVF and NM groups were defined with stringent cutoffs (fold change >4 & p.adj <0.01) using DESeq2, and the genes with low expression (maximum gene expression ≤ 2) were discarded. The differentially imprinted genes in Figures S2B for the IVF and NM groups were defined with stringent cutoffs (fold change >4 & p.adj <0.01) using DESeq2, and the genes with low expression (maximum gene expression ≤ 2) were discarded. The lineage-specific genes in Figure 3A for the NM group were defined with stringent cutoffs (fold change >4 & p.adj <0.01) using DESeq2. Genes with maximum expression values > 2 (normalized read counts >3) and genes with large variances among biological replicates were discarded. The Epi-specific TFs and ExE-specific TFs in Figure 3B are subsets of the lineage-specific genes in Figure 3A, and their expression satisfied either of the following pairs of criteria: log2CPM >3 in Epi & log2CPM <2 in ExE or log2CPM >3 in ExE & log2CPM <2 in Epi.

Gene Ontology (GO) analysis

GO analysis of the DEGs was performed with Metascape (Zhou et al., 2019).

QUANTIFICATION AND STATISTICAL ANALYSIS

The statistics were performed using GraphPad Prism. The statistical details of the data described in this paper, including the statistical tests used, the value and definition of n, and dispersion and precision measures, can be found in the figure legends.